© 2015. Published by The Company of Biologists Ltd | Development (2015) 142, 3833-3844 doi:10.1242/dev.126003

RESEARCH ARTICLE

De novo DNA methylation through the 5′-segment of the *H19* ICR maintains its imprint during early embryogenesis

Hitomi Matsuzaki[1,2], Eiichi Okamura[3], Takuya Takahashi[3], Aki Ushiki[3], Toshinobu Nakamura[4], Toru Nakano[5], Kenichiro Hata[6], Akiyoshi Fukamizu[1,2] and Keiji Tanimoto[1,2,*]

ABSTRACT

Genomic imprinting is a major monoallelic gene expression regulatory mechanism in mammals, and depends on gamete-specific DNA methylation of specialized *cis*-regulatory elements called imprinting control regions (ICRs). Allele-specific DNA methylation of the ICRs is faithfully maintained at the imprinted loci throughout development, even in early embryos where genomes undergo extensive epigenetic reprogramming, including DNA demethylation, to acquire totipotency. We previously found that an ectopically introduced *H19* ICR fragment in transgenic mice acquired paternal allele-specific methylation in the somatic cells of offspring, whereas it was not methylated in sperm, suggesting that its gametic and postfertilization modifications were separable events. We hypothesized that this latter activity might contribute to maintenance of the methylation imprint in early embryos. Here, we demonstrate that methylation of the paternally inherited transgenic *H19* ICR commences soon after fertilization in a maternal DNMT3A- and DNMT3L-dependent manner. When its germline methylation was partially obstructed by insertion of insulator sequences, the endogenous paternal *H19* ICR also exhibited postfertilization methylation. Finally, we refined the responsible sequences for this activity in transgenic mice and found that deletion of the 5′ segment of the endogenous paternal *H19* ICR decreased its methylation after fertilization and attenuated *Igf2* gene expression. These results demonstrate that this segment of the *H19* ICR is essential for its *de novo* postfertilization DNA methylation, and that this activity contributes to the maintenance of imprinted methylation at the endogenous *H19* ICR during early embryogenesis.

KEY WORDS: DNA methylation, Genomic imprinting, *Igf2*/*H19* locus, Early embryogenesis

INTRODUCTION

Genomic imprinting is an epigenetic phenomenon in mammals that causes parental-specific, monoallelic expression of a subset of autosomal genes. The unique expression patterns of imprinted genes are controlled by allele-specific DNA methylation of the *cis*-regulatory sequences, called the imprinting control regions (ICRs). Because allelic DNA methylation of ICRs is acquired during gametogenesis, ICRs are also called germline differentially methylated regions (gDMRs) (Ferguson-Smith, 2011; Kelsey and Feil, 2013; Tomizawa and Sasaki, 2012). Recent genome-wide profiling has, however, revealed that the number of oocyte- or sperm-specific methylated genomic regions is far more than that of the known ICRs (Kobayashi et al., 2012; Smallwood et al., 2011). Therefore, germline methylation might not be restricted to ICRs, and both the ICRs and the other gDMRs could be methylated by a common mechanism without being strictly discriminated in the germ line (Kelsey and Feil, 2013).

During preimplantation development, although most gDMRs lose their gamete-derived methylation via epigenetic reprogramming activity, allelic methylation of ICRs is faithfully maintained (Kobayashi et al., 2012; Smallwood et al., 2011). Presumably, the methylation maintenance mechanism against genome-wide demethylation activity might operate at restricted genomic loci and selected alleles in preimplantation embryos. We and others have reported that Stella (also known as DPPA3) (Nakamura et al., 2007), KAP1 (also known as TRIM28) (Messerschmidt et al., 2012), and NuRD complex components (Ma et al., 2010; Reese et al., 2007), in addition to the maintenance methyltransferase DNMT1 (Hirasawa et al., 2008), help to maintain ICR methylation in preimplantation embryos. Because these factors have no sequence specificity for DNA binding or intrinsic DNA binding ability themselves, other sequence-specific DNA binding proteins must be required for their recruitment to specific target sites. The Krüppel-associated box (KRAB)-containing zinc-finger protein ZFP57, which was found to interact with KAP1, is a dominant candidate for such a protein (Li et al., 2008; Messerschmidt et al., 2012; Quenneville et al., 2011). However, because the depletion of ZFP57 did not always affect the methylation of ICRs (Li et al., 2008), other factors and their target *cis* elements are apparently engaged in the maintenance mechanism.

The *H19* ICR in the mouse *Igf2/H19* locus (Fig. 1A) is DNA-methylated by the DNMT3A-DNMT3L complex in prospermatogonia, the status of which is maintained on the paternal allele following fertilization (Kaneda et al., 2004; Tremblay et al., 1997), and it is thus classified as a gDMR. Whereas indispensable roles for CTCF (Matsuzaki et al., 2010; Schoenherr et al., 2003) and Sox-Oct binding motifs (Sakaguchi et al., 2013; Zimmerman et al., 2013) in maintaining maternal *H19* ICR hypomethylation during postimplantation periods are well established, little is known about the underlying mechanisms that maintain paternal *H19* ICR hypermethylation during preimplantation periods.

We previously tested the activity of the *H19* ICR in yeast artificial chromosome (YAC) transgenic mice (TgM), in which an *H19* ICR fragment (2.9 kb) was inserted into a YAC bearing the (nonimprinted) human β-globin locus (150 kb, Fig. 1B) to minimize position effects of transgene insertion sites (Tanimoto

[1]Faculty of Life and Environmental Sciences, University of Tsukuba, Tsukuba, Ibaraki 305-8577, Japan. [2]Life Science Center of Tsukuba Advanced Research Alliance (TARA), University of Tsukuba, Tsukuba, Ibaraki 305-8577, Japan. [3]Graduate School of Life and Environmental Sciences, University of Tsukuba, Tsukuba, Ibaraki 305-8577, Japan. [4]Department of Animal Bio-Science, Nagahama Institute of Bio-Science and Technology, Nagahama, Shiga 526-0829, Japan. [5]Graduate School of Frontier Biosciences, Osaka University, Suita, Osaka 565-0871, Japan. [6]Department of Maternal-Fetal Biology, National Research Institute for Child Health and Development, Setagaya, Tokyo 157-8535, Japan.

*Author for correspondence (keiji@tara.tsukuba.ac.jp)

Received 2 May 2015; Accepted 15 September 2015

Development (2015) 142, 3833-3844 doi:10.1242/dev.126003

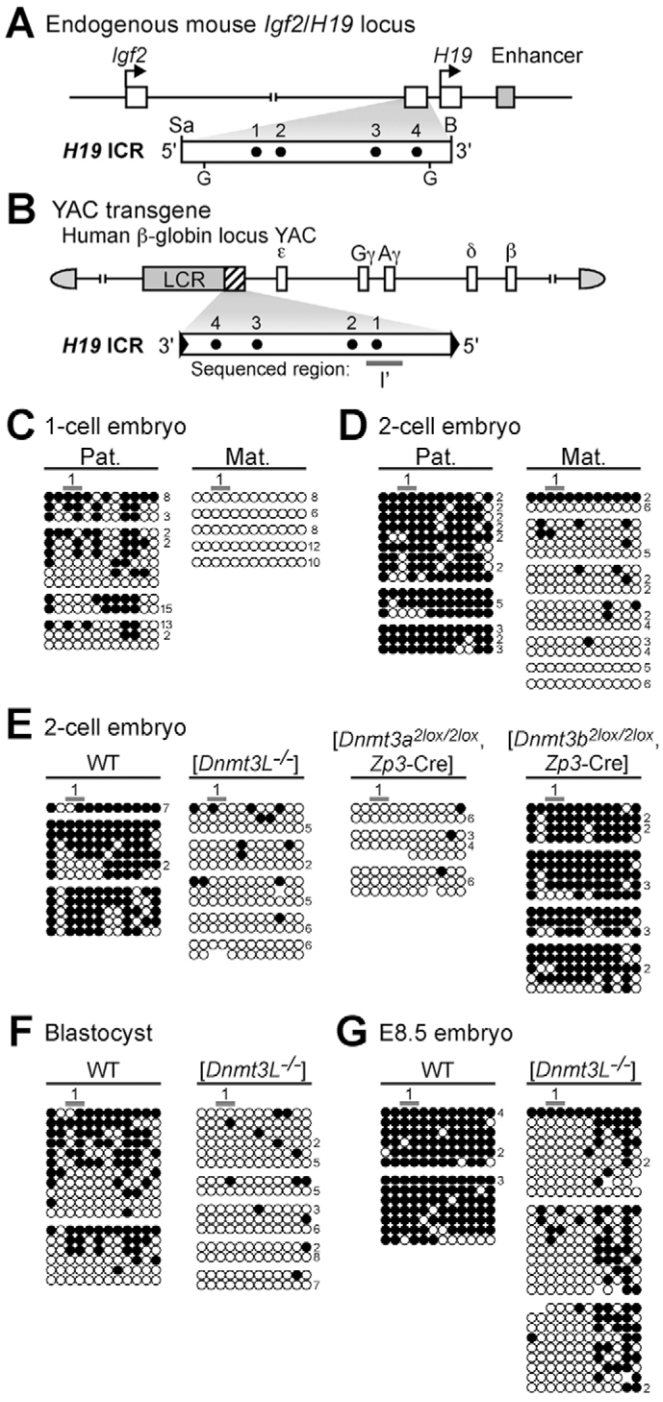

Fig. 1. DNA methylation status of the transgenic *H19* ICR in early embryos. (A) Structure of the mouse *Igf2*/*H19* locus. Mouse *Igf2* and *H19* (open boxes) are ∼90 kb apart, and the expression of both genes depends on the shared 3′ enhancer (gray box). The *H19* ICR, located approximately at −4 to −2 kb relative to the transcription start site of *H19* is contained within a 2.9-kb *Sac*I (Sa)-*Bam*HI (B) fragment. Dots (1-4) indicate the position of CTCF binding sites. G; *Bgl*II site. (B) Structure of the ICR/β-globin YAC transgene. The 150-kb human β-globin locus YAC carries the LCR (gray box) and the β-like globin genes (open boxes). The 2.9-kb *H19* ICR fragment (inverted orientation) was introduced between the LCR and the ε-globin gene (Tanimoto et al., 2005). A gray bar below the map indicates sequences (region I′) analyzed by bisulfite sequencing. (C,D) Methylation status of the transgenic *H19* ICR in embryos. One- (C) or two-cell (D) embryos that inherited the ICR/β-globin YAC transgene (line 1048) either paternally (Pat.) or maternally (Mat.) were embedded in agarose beads (19-43 embryos per bead in C, 13-37 embryos per bead in D) and treated with sodium bisulfite. The beads were separately and directly used to amplify the region I′ of the transgenic *H19* ICR by nested PCR. PCR products were individually subcloned and sequenced. The results from single beads are presented together in a cluster. Each horizontal row represents a single DNA template molecule. The numbers on the right of each row indicate number of times the pattern was observed in the sequencing. Methylated and unmethylated CpG motifs are shown as filled and open circles, respectively. (E,F) A role of *de novo* DNA methyltransferases in the postfertilization methylation of the paternally inherited transgenic *H19* ICR. Two-cell (E) or blastocyst (F)-stage embryos were obtained from wild-type (WT), [*Dnmt3l* $^{-/-}$], [*Dnmt3a*$^{2lox/2lox}$, *Zp3-Cre*], or [*Dnmt3b*$^{2lox/2lox}$, *Zp3-Cre*] females crossed with the ICR/β-globin male TgM carrying WT Dnmts (5-24 embryos in E, 1-9 embryos in F). The methylation status of the paternally inherited transgenic *H19* ICR (region I′) was analyzed by bisulfite sequencing as described previously. (G) E8.5 embryos were obtained from WT or [*Dnmt3l*$^{-/-}$] females crossed with ICR/β-globin male TgM. Genomic DNA was extracted from each embryo and treated with sodium bisulfite, and region I′ of the transgenic *H19* ICR was amplified by nested PCR. PCR products were subcloned and sequenced. The results from single embryos are presented together in a cluster. Above each panel in E-G are genotypes of mothers.

et al., 2005). In somatic cells, the *H19* ICR fragment was preferentially methylated when paternally inherited, demonstrating that the 2.9-kb sequence contained sufficient information to recapitulate imprinted methylation. Surprisingly, however, the transgenic *H19* ICR was not methylated in the testes. In addition, randomly integrated *H19* ICR fragments in the mouse genome were hypermethylated in the paternal allele after fertilization, irrespective of their variable methylation levels in the testes of multiple TgM lines (Matsuzaki et al., 2009). It was therefore presumed that the *H19* ICR was marked by an epigenetic modification other than DNA methylation in the germ line, and that paternal allele-specific methylation was acquired after fertilization by referring to this hypothetical mark. Hence, our results and those of others (Gebert et al., 2010; Park et al., 2004) suggested that two distinct methylation mechanisms operate at the endogenous *H19* ICR: one in the germ line, which is under the control of its surrounding sequences, and the other during the postfertilization period, which is governed by a hypothetical epigenetic mark preset within the *H19* ICR during gametogenesis. We speculated that the latter activity might be actively involved in the region-specific maintenance of allelic methylation at the endogenous *H19* ICR in preimplantation embryos.

In this study, we show that the paternal-allele-specific methylation of the transgenic *H19* ICR commences soon after fertilization in YAC-TgM, and that maternally supplied DNMT3A and DNMT3L are required for this process. By partially obstructing germline methylation of the endogenous *H19* ICR, we discovered that postfertilization methylation activity also exists at the endogenous *H19* ICR. Furthermore, in YAC-TgM, we substantially narrowed the responsible sequences for postfertilization methylation acquisition in the transgenic *H19* ICR. Finally, by deleting the responsible sequences from the endogenous locus, we noted a partial loss of methylation in the paternally inherited *H19* ICR after fertilization, diminished *Igf2* expression, and embryonic growth retardation in the offspring that paternally inherited the mutation. These results demonstrate that the postfertilization methylation imprinting activity of the *H19* ICR is essential for maintaining its imprinted methylation status once established during gametogenesis.

RESULTS

Methylation acquisition at the transgenic *H19* ICR in early embryos

The *H19* ICR fragment inserted into the β-globin YAC transgene (Fig. 1B) exhibited preferential DNA methylation in the somatic cells of offspring after paternal transmission, whereas it was not

Development (2015) 142, 3833-3844 doi:10.1242/dev.126003

methylated in sperm (Fig. S1A-C) (Tanimoto et al., 2005). As a first step in elucidating the mechanism of the allele-specific methylation of the transgenic *H19* ICR, we examined the timing of its acquisition in mouse early embryos. Bisulfite sequencing of the transgenic *H19* ICR (region I′ including the CTCF site 1, Fig. 1B) revealed that the paternally inherited ICR was moderately and heavily methylated in one- and two-cell stage embryos, respectively (Fig. 1C,D, Fig. S1D), the levels of which were substantially higher than in the maternally inherited alleles. While the DNA methylation level in region I′ in two-cell embryos was already high (Fig. 1D, Fig. S1D) and indistinguishable from that in blastocyst-stage embryos (Fig. S1E) (Matsuzaki et al., 2010), DNA methylation around CTCF binding site 4 of the paternally inherited *H19* ICR was low in blastocysts (region II, Fig. S1F), suggesting that DNA methylation acquisition directionally extends from a region near CTCF site 1. These results suggested that the paternally inherited transgenic *H19* ICR is recognized by the DNA methylation machinery soon after fertilization and becomes progressively methylated during embryonic development.

A role for DNMT3s in the postfertilization methylation of the transgenic *H19* ICR

Methylation acquisition in the endogenous *H19* ICR occurs in fetal prospermatogonia via the actions of DNMT3A and DNMT3L (Kaneda et al., 2004). However, the activity and targets, if any, of the DNMT3 family in early embryos remain obscure. We thus examined which DNMTs were involved in methylation acquisition in the transgenic *H19* ICR. Because the gene products present in early embryos soon after fertilization are mostly derived from oocytes, we assessed the roles of DNMTs on postfertilization methylation of the transgenic *H19* ICR after maternal disruption. To test the function of *Dnmt3l*, *Dnmt3l*-null (−/−) (Hata et al., 2002) females were mated with ICR/β-globin YAC transgenic (*Dnmt3l* wild-type) (Fig. 1B) (Tanimoto et al., 2005) males. Because $Dnmt3a^{-/-}$ or $Dnmt3b^{-/-}$ mice are not viable (Okano et al., 1999), we used Cre-loxP recombination to specifically eliminate these genes in growing oocytes via the *zona pellucida glycoprotein 3* (*Zp3*) promoter-*Cre* transgene (de Vries et al., 2000; Dodge et al., 2005; Kaneda et al., 2004). After confirming that *Dnmt3* gene products were depleted in both oocytes and early embryos by quantitative reverse transcription-polymerase chain reaction (RT-qPCR) (Fig. S2), we analyzed the methylation status of the transgenic *H19* ICR fragment. In *Dnmt3l*-deficient two-cell embryos, the paternally inherited transgenic *H19* ICR was hypomethylated (Fig. 1E). Depletion of maternally provided *Dnmt3a* gene product also caused hypomethylation of the transgenic *H19* ICR, whereas the loss of the *Dnmt3b* gene product did not affect its methylation (Fig. 1E). These results demonstrated that the postfertilization methylation acquisition of the paternally inherited transgenic *H19* ICR required both DNMT3A and DNMT3L, which were maternally provided to early embryos.

We next examined whether zygotic expression of Dnmts (Fig. S2) (Guenatri et al., 2013; Hu et al., 2008) would compensate for a loss of maternally provided DNMT3L in transgenic *H19* ICR methylation during embryogenesis. The paternally inherited transgenic *H19* ICR remained unmethylated in blastocyst-stage embryos derived from $Dnmt3l^{-/-}$ mothers (Fig. 1F). The unmethylated state of the transgenic *H19* ICR did not change even at embryonic day (E) 8.5, despite the fact that allele-nonspecific methylation, probably elicited by postimplantation *de novo* DNA methylation activity, was observed outside of the DMR (Fig. 1G) (Matsuzaki et al., 2010). These results demonstrated that the paternally inherited transgenic *H19* ICR must be recognized by the DNA methylation machinery, including DNMT3A and DNMT3L, in early embryos to acquire imprinted methylation.

Evaluation of the postfertilization methylation activity at the endogenous *H19* ICR

Although the transgenic *H19* ICR possesses intrinsic activity to acquire paternal allele-specific methylation in early embryos, it is unclear whether this activity also exists at the endogenous locus. Because the endogenous *H19* ICR is fully methylated in sperm, the postfertilization methylation activity at the endogenous locus, if present, is normally difficult to reveal. Our previous results (Matsuzaki et al., 2009) and those of others (Gebert et al., 2010; Park et al., 2004; Puget et al., 2015) suggested that the gametic methylation of the *H19* ICR was governed by signals from surrounding sequences, i.e. those located outside the 2.9-kb *H19* ICR region. Therefore, by interfering with the transmission of these hypothetical signals and subsequent methylation during spermatogenesis, we sought to verify the postfertilization methylation imprinting activity at the endogenous locus. To this end, we inserted tandemly arrayed chicken HS4 core sequences, $(cHS4c)_2$,on both sides of the endogenous *H19* ICR (Fig. 2A), expecting that this would block a presumptive signal to direct DNA methylation of the *H19* ICR in the germ line, as the cHS4 itself was unmethylated in both germ and somatic cells when it was substituted for the endogenous *H19* ICR (Szabo et al., 2002). Importantly, during the postfertilization period, the same manipulation does not prevent methylation imprinting activity in the context of YAC-TgM (Okamura et al., 2013a). Embryonic stem cells (ESCs) were modified by homologous recombination, and accurate targeting events were confirmed by Southern blotting (Fig. S3A,B). Following the establishment of two knock-in mouse lines (Fig. S3B), the neo^r selectable marker was excised by mating them with Cre-expressing TgM (Fig. S3C).

Germline methylation of the endogenous *H19* ICR is inhibited by flanking insulator sequences

We examined the methylation status of the insulated *H19* ICR allele in sperm by bisulfite sequencing. The $(cHS4c)_2$ sequences on both sides of the *H19* ICR were hypomethylated (Fig. 2B). In addition, the *H19* ICR region containing CTCF sites 3 and 4 was also methylated at very low levels. Furthermore, the region around the CTCF sites 1 and 2 was significantly less methylated (Fig. 2B) in comparison to the fully methylated sequences in the wild-type allele (Fig. S3D) ($P<0.0001$, Mann–Whitney U-test; http://quma.cdb.riken.jp/). Southern blotting using methylation-sensitive restriction enzymes confirmed these results (Fig. S4A,B). These results indicated that the flanking $(cHS4c)_2$ fragments at the endogenous *H19* ICR inhibited its methylation acquisition during spermatogenesis. It was reported that USF1 binding to cHS4 sequences induces histone H3/H4 acetylation and H3K4 methylation, thereby interfering with the spread of repressive histone modifications (such as H3K9 methylation) and heterochromatin formation (West et al., 2004). We therefore infer that intrusion of the repressive chromatin state into the *H19* ICR from outside might be a prerequisite for its gametic methylation and that flanking cHS4c might block this process. Alternative hypotheses might be that VEZF1-bound cHS4c sequences or simply its CpG island-like nature somehow interfered with the *de novo* DNA methylation of the neighboring *H19* ICR only during spermatogenesis (Dickson et al., 2010; Kobayashi et al., 2012; Smallwood et al., 2011). It is also possible that cHS4c

Development (2015) 142, 3833-3844 doi:10.1242/dev.126003

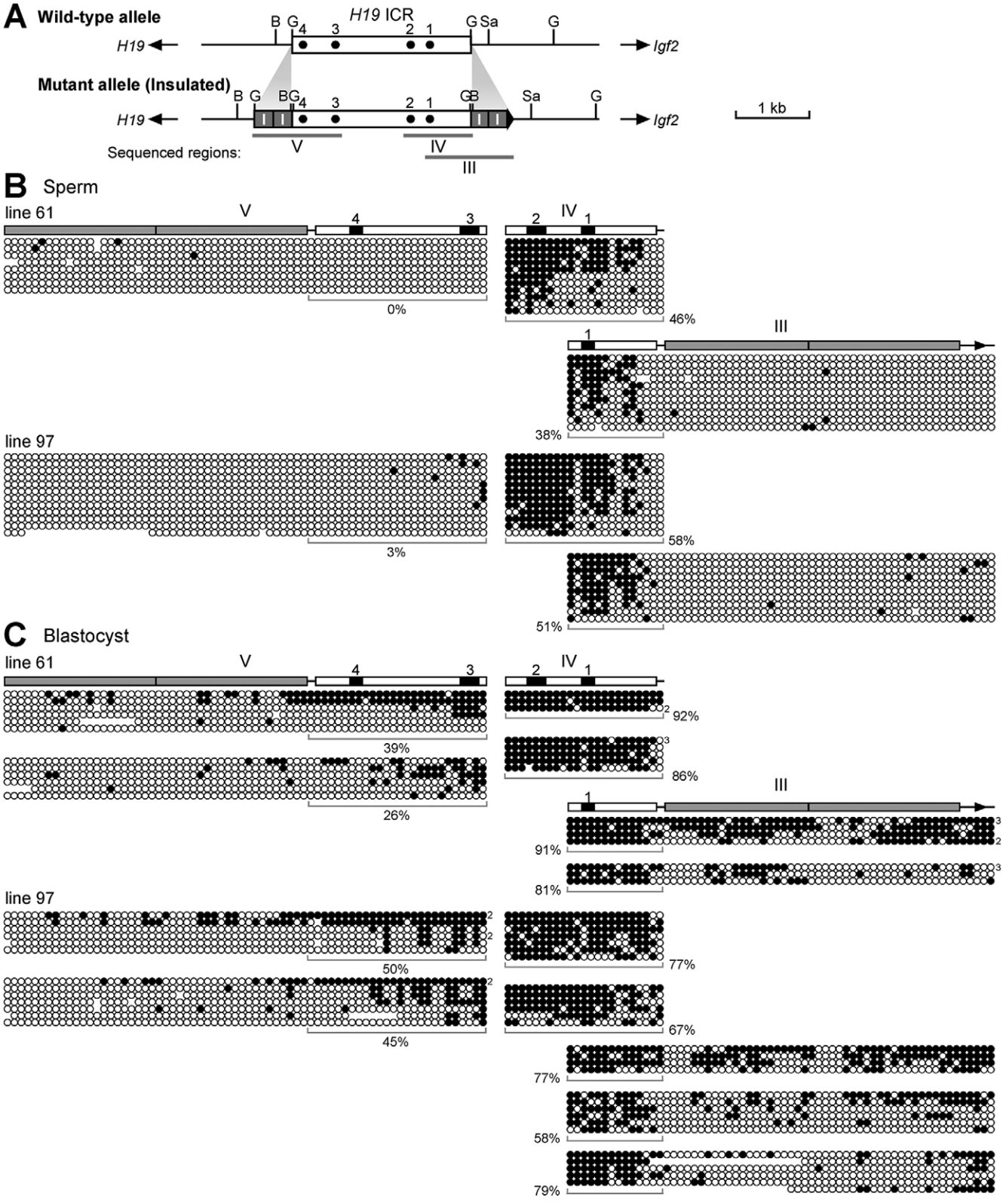

Fig. 2. DNA methylation status of the insulated *H19* ICR in sperm and blastocysts. (A) Map of the wild-type and mutant *H19* loci. Tandem cHS4 core fragments (gray rectangles, I for insulator) were inserted at both sides of the *H19* ICR [at *Bgl*II (G) sites: mutant allele] (see also Fig. S3). Three regions of the mutant allele (III, IV, and V; gray bars beneath the map) were analyzed by bisulfite sequencing in B and C. B, *Bam*HI; Sa, *Sac*I sites; dots 1-4, CTCF binding sites. (B) Genomic DNA extracted from sperm of mutant mice (lines 61 and 97) was digested with *Xba*I and treated with sodium bisulfite. Three regions of the mutant allele were amplified by PCR, subcloned, and sequenced. The overall percentage of methylated CpGs in region IV or those in the ICR portions of region III or V are indicated next to each panel. (C) Blastocyst-stage embryos that inherited the mutant allele paternally were embedded in agarose beads (6-12 embryos per bead) and treated with sodium bisulfite. The beads were used for amplifying three regions of the mutant allele by PCR, and the resulting fragments were individually subcloned and sequenced.

Development (2015) 142, 3833-3844 doi:10.1242/dev.126003

sequences interfered with transcription read-through at the *H19* ICR, which has been suggested to induce its methylation in male germ cells (Henckel et al., 2012).

Allele-specific postfertilization DNA methylation at the insulated *H19* ICR

We next examined the methylation status of the insulated *H19* ICR after fertilization. In blastocyst-stage embryos (Fig. 2C), as well as in the somatic cells of neonates (Fig. S4A,C-E), the paternally inherited insulated *H19* ICR exhibited higher methylation levels than those observed in sperm (Fig. 2B). The markedly elevated level of methylation in $(cHS4c)_2$ sequences on the paternal allele (Fig. S4E) was probably a secondary consequence of imprinted methylation of the adjacent *H19* ICR as the same sequences were unmethylated after maternal transmission. These results demonstrated that the endogenous *H19* ICR was methylated after fertilization in a paternal allele-specific manner, and that the methylation acquisition commenced during the preimplantation period.

In the YAC-TgM, transgenic *H19* ICR methylation in early embryos was dependent on maternally provided DNMT3L and DNMT3A (Fig. 1E,F). We therefore examined whether the same DNA methyltransferases were operating at the endogenous insulated *H19* ICR. When *Dnmt3l* $^{-/-}$ female mice were bred, the paternally inherited insulated *H19* ICR region (region IV in Fig. 3A) was less methylated in blastocyst (Fig. 3B) than in control embryos (WT), indicating that DNMT3L is involved in the methylation of the endogenous *H19* locus. In addition, the effect of maternal DNMT3L depletion on the postfertilization methylation at the endogenous insulated *H19* ICR was observed in as early as 2-cell embryos (Fig. 3C), the same timing when postfertilization methylation acquisition took place in the YAC TgM (Fig. 1D).

Taken together, these results suggest that postfertilization paternal allele-specific methylation activity also exists in the endogenous *H19* ICR, which is probably governed by a shared mechanism with the transgenic *H19* ICR.

Defining the *H19* ICR DNA sequences essential for allele-specific postfertilization DNA methylation in YAC-TgM

To further elucidate the mechanisms underlying the postfertilization methylation of the *H19* ICR, we sought to more precisely define its responsive sequences. To this end, we employed a YAC-TgM system, in which the methylation activity is clearly detectable after fertilization because of its unmethylated state in sperm. We previously demonstrated that the 1.7-kb 'ICR21' fragment covering CTCF sites 1 and 2 (Fig. 4A) was sufficient to recapitulate paternal allele-specific DNA methylation after fertilization in YAC-TgM (Okamura et al., 2013b). We thus generated a series of 5′-truncated *H19* ICR fragments: the ICR4321S fragment, in which the 5′-end of the 2.9-kb *H19* ICR fragment (766 bp) was deleted but all four CTCF sites remained; and the ICR432 fragment, which is 173 bp shorter than the ICR4321S fragment and lacks CTCF site 1 (Fig. 4A). To reduce the time required to obtain mouse lines carrying intact single-copy YAC transgenes, these two fragments were individually floxed using hetero-specific *loxP* sequences, combined to employ a co-placement strategy (Tanimoto et al., 2008), and introduced 3′ to the locus control region (LCR) in the human β-globin YAC (Fig. S5A). YAC-TgM were generated by pronuclear injection and intact, single-copy transgene carriers were identified (Fig. S5A,B). Parental YAC-TgM lines (Numbers 443 and 429) were crossed with Cre-TgM to initiate *in vivo* Cre-loxP recombination, which generated daughter lines carrying either the ICR4321S or ICR432

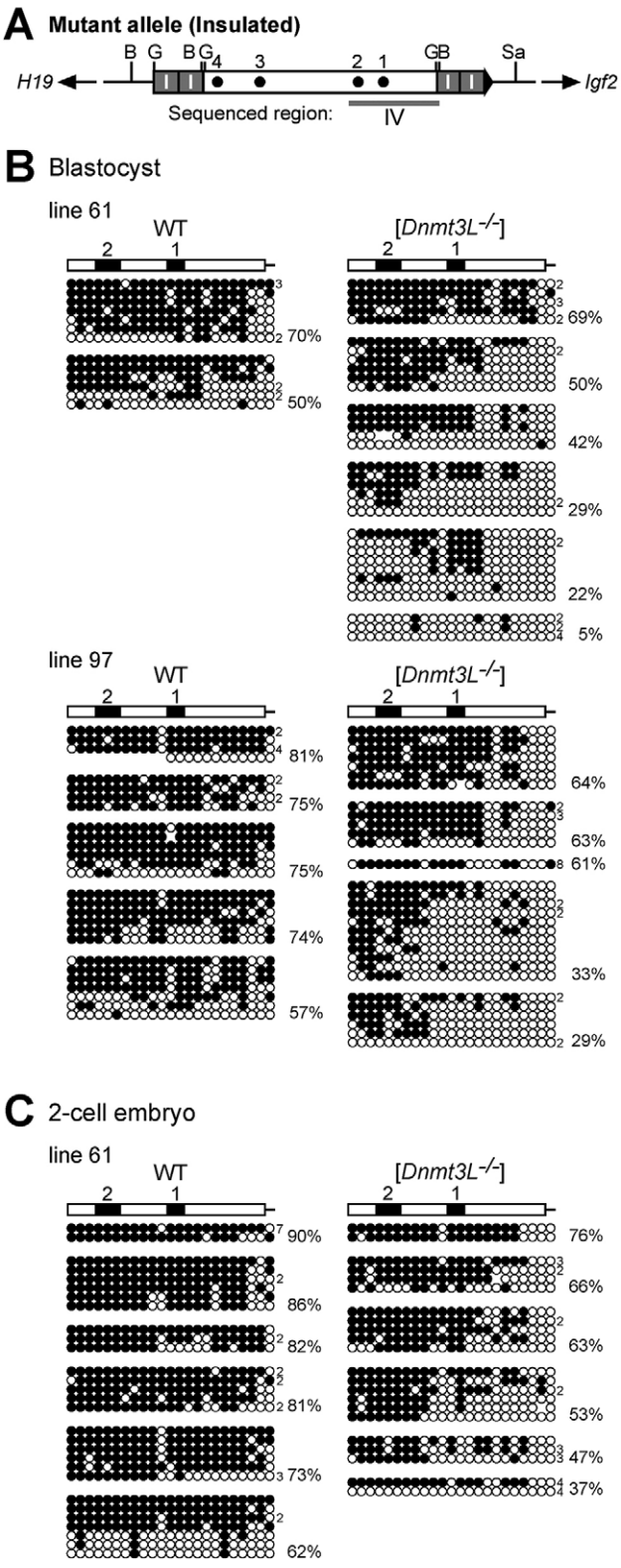

Fig. 3. Function of DNMT3L in postfertilization methylation of the paternally inherited insulated *H19* ICR. Blastocyst (lines 61 and 97) and 2-cell (line 61) stage embryos were obtained from wild-type (WT) or [*Dnmt3l*$^{-/-}$] females crossed with male mice carrying mutant (insulated) *H19* ICR allele. DNA methylation status of region IV (shown in A, map legend as per Fig. 2A) of the paternally inherited mutant allele was analyzed by bisulfite sequencing, as described above, for blastocyst- (B) and 2-cell stage embryos (C). Three to 10 (blastocyst) or 13 to 30 (2-cell) embryos per agarose bead were used. Above each panel in B and C are genotypes of mothers.

Development (2015) 142, 3833-3844 doi:10.1242/dev.126003

transgene at the identical chromosomal integration site (Fig. 4B, Fig. S5C,D).

We examined the methylation status of the transgene fragments in somatic cells by Southern blotting (Fig. 4C). The ICR4321S fragment was hypomethylated regardless of its parental origin (Fig. 4D). The methylation status was also determined by bisulfite sequencing. Region VII, covering CTCF sites 3 and 4 (Fig. 5A), was hypomethylated regardless of parental origin (Fig. 5B). Although region VI, containing CTCF sites 1 and 2 (Fig. 5A), was partially methylated, its overall methylation level was low and equally observed on both alleles, implying that this methylation acquisition was allele-nonspecific (Fig. 5B). Because hypomethylation of the paternally inherited ICR4321S fragment was also observed in two-cell embryos (Fig. 5C), it is suggested that the ICR4321S fragment lost its ability to acquire *de novo* DNA methylation in the early embryo. As was seen in the wild-type 2.9-kb *H19* ICR TgM (Fig. S1B,C) (Tanimoto et al., 2005), the ICR4321S fragment was not methylated in testis (Fig. S6E), indicating that the deleted sequence was not involved in methylation regulation of the *H19* ICR in male germ cells. Essentially the same phenotype, i.e. hypomethylation on both parental alleles in somatic cells (Fig. S6A-C) and in male germ cells (Fig. S6D), was observed in the shorter ICR432 fragment TgM. These results demonstrated that the 5′-region of the *H19* ICR is necessary for postfertilization allele-

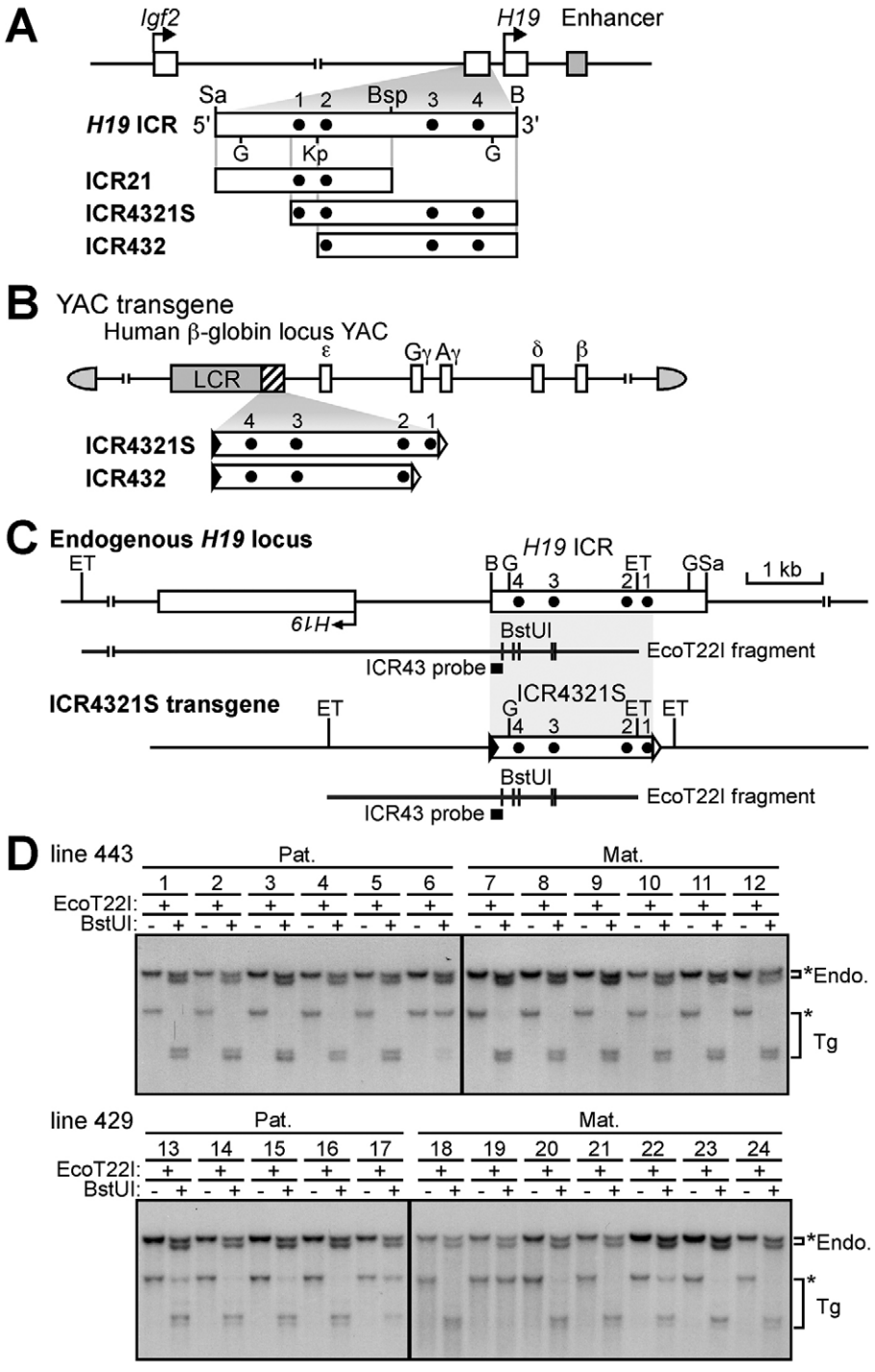

Fig. 4. Generation and DNA methylation analysis of the YAC-TgM carrying the 5′-truncated *H19* ICR fragments. (A) Schematic representation of the *H19* ICR, ICR21 (Okamura et al., 2013b), ICR4321S, and ICR432 DNA fragments. Sa, *Sac*I; B, *Bam*HI; Bsp, *Bsp*EI; G, *Bgl*II; Kp, *Kpn*I sites; dots 1-4, CTCF binding sites. (B) The ICR4321S and ICR432 fragments were inserted 3′ to the LCR in the human β-globin YAC, and YAC-TgM were generated (see also Fig. S5). (C) Partial restriction enzyme maps of the endogenous *H19* locus and the β-globin YAC transgene with the inserted ICR4321S fragment. Methylation-sensitive *Bst*UI sites in the *Eco*T22I (ET) fragments are displayed as vertical lines beneath each map. The ICR43 probe used for Southern blotting in D is shown as a filled rectangle. (D) DNA methylation status of the ICR4321S fragment in somatic cells of the YAC-TgM (lines 443 and 429) that inherited the transgenes either paternally (Pat.) or maternally (Mat.). Tail DNA was digested with *Eco*T22I and then *Bst*UI, and the blot was hybridized with the ICR43 probe. Endo., endogenous locus; Tg, transgene. Asterisks indicate the positions of parental or methylated undigested fragments.

Development (2015) 142, 3833-3844 doi:10.1242/dev.126003

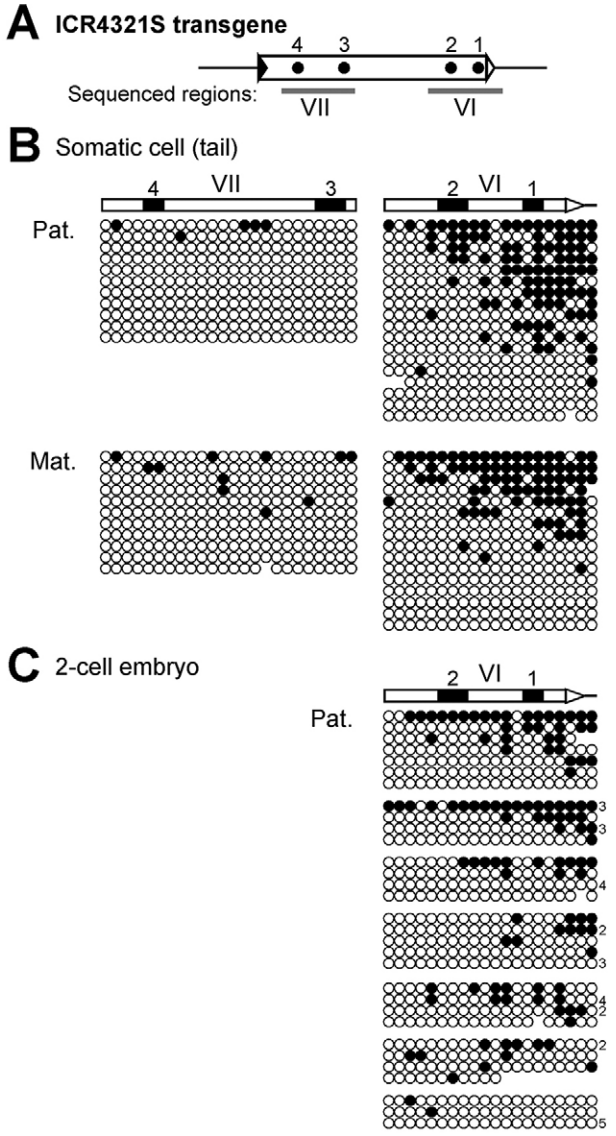

Fig. 5. DNA methylation status of the ICR4321S transgene in tail somatic cells and preimplantation embryos. (A) Map of the ICR4321S fragment. Two regions (VI and VII) analyzed by bisulfite sequencing in B and C are shown as gray bars beneath the map. (B) DNA methylation status of regions VI and VII in somatic cells of the ICR4321S YAC-TgM (line 443) that inherited the transgenes either paternally (Pat.) or maternally (Mat.). Tail DNA was digested with *Xba*I and treated with sodium bisulfite. Two regions were amplified by nested PCR, subcloned, and sequenced. (C) The DNA methylation status of region VI in 2-cell embryos that inherited the ICR4321S YAC transgene paternally (Pat.) (line 443) was analyzed by bisulfite sequencing as described previously. 16-38 embryos per bead were used.

specific methylation acquisition, which commences during early embryogenesis, in YAC-TgM.

The role of the 5′-region of the *H19* ICR in allele-specific methylation at the endogenous locus

To elucidate whether the 5′-end of the *H19* ICR was also essential for its allele-specific methylation at the endogenous locus, we removed a 765-bp sequence, which we deleted in the ICR4321S fragment, from the endogenous *H19* ICR (Fig. 6A, Fig. S7). ESCs were transformed with the targeting vector, in which the 765-bp sequence was flanked by *loxP* sequences (Fig. S7A). Properly targeted ESCs were identified by Southern blotting and used for generating a knock-in mouse line (Fig. S7B). The 765-bp sequence and neo^r selectable marker were simultaneously excised from the parental allele by crossing with Cre-expressing TgM, and the precise recombination events were monitored by Southern blotting (5′ICR-KO allele; Fig. S7C).

We first examined the methylation status of the paternally inherited 5′ICR-KO allele in somatic cells (tail tips) of the mutant mice by Southern blotting. The methylation levels of the remaining *H19* ICR sequences were partially reduced in more than half of the offspring (Fig. 6A,B). To further clarify the methylation status, we conducted bisulfite sequencing analysis of the DNA region covering CTCF sites 1 and 2. Based on the Southern blotting results (Fig. 6B), DNA samples from mutant mice carrying highly (numbers 1 and 2) and partially (numbers 3-8 and 9-13) methylated paternally inherited knock out (KO) alleles were individually pooled and subjected to analysis. Consistent with the Southern blotting data, some sequenced clones exhibited partial loss of methylation, particularly around the internal region of the residual *H19* ICR. By contrast, the wild-type paternal allele was fully methylated (Fig. 6C). To explore the reason behind the diminished methylation on the paternal KO allele, we conducted methylation analysis of sperm and preimplantation embryos (1-cell, 2-cell and blastocyst stages). Although the KO allele was fully methylated in sperm (Fig. 6D), the paternally inherited KO allele exhibited a partial loss of methylation even in 1-cell stage embryos (Fig. 6E). These results suggested that the 5′-region of the *H19* ICR was essential for its *de novo* DNA methylation at the endogenous, as well as at the transgene loci, in early embryos, and contributed to ensuring the maintenance of differential methylation during this developmental period.

The partial loss of methylation on the paternal KO allele was also observed in E12.5 embryos (Fig. 7A). Because the *H19* ICR methylation status regulates *Igf2* and *H19* transcription (Bell and Felsenfeld, 2000; Hark et al., 2000; Srivastava et al., 2000), we analyzed the expression of these genes. The expression levels of *Igf2* and *H19* were decreased and increased, respectively, in the livers of E12.5 embryos inheriting the KO allele paternally, when compared with littermate controls (Fig. 7B). Importantly, the degree of methylation loss at the *H19* ICR in each embryo correlated highly with the change in gene expression levels. While the product of *Igf2* promotes fetal growth (DeChiara et al., 1991), that of *H19* [non-coding RNA, carrying a micro RNA (miR-675) sequence] has been proposed to act as a growth repressor (Gabory et al., 2010). In accordance with the expected functions of these genes, the embryos (E12.5) carrying a paternally inherited KO allele tended to be smaller than control embryos from the same litter (Fig. S8). These results suggested that the 5′-region of the *H19* ICR played an essential role in normal *Igf2/H19* expression and fetal growth through the maintenance of paternal allele-specific methylation status after fertilization.

DISCUSSION

Using a genetic strategy, we found that maternally supplied DNMT3A and DNMT3L enzymes are essential for the *de novo* DNA methylation of the paternally inherited transgenic *H19* ICR in preimplantation embryos (Fig. 1E). Even in the presence of these enzymes (Fig. S2) (Guenatri et al., 2013; Hirasawa et al., 2008), the maternally inherited transgenic (Fig. 1C,D) and endogenous *H19* ICRs do not acquire methylation. Therefore, it was strongly suggested that an epigenetic mark other than DNA methylation is set within the transgenic *H19* ICR during gametogenesis, and after fertilization, the mark is used for discriminating the parental alleles

Development (2015) 142, 3833-3844 doi:10.1242/dev.126003

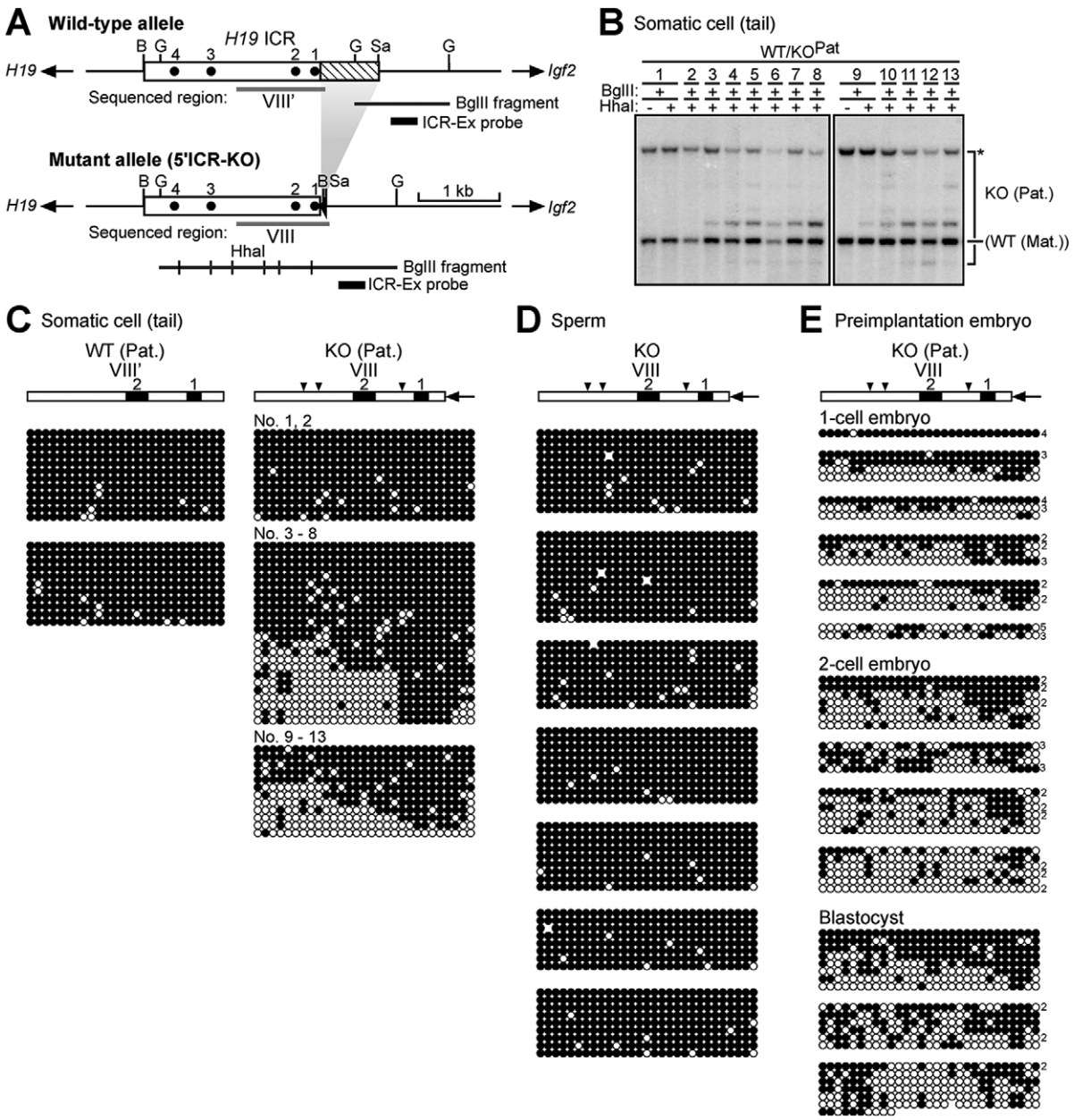

Fig. 6. DNA methylation status of the 5′-deleted endogenous *H19* ICR. (A) Map of the wild-type and mutant *H19* gene loci. The *H19* ICR 5′-region (765 bp, shaded area) was excised from the endogenous locus (mutant allele 5′ICR-KO; see also Fig. S7). Methylation-sensitive *Hha*I sites in the *Bgl*II (G) fragment are displayed as vertical lines beneath the mutant allele map. The ICR-Ex probe used for Southern blotting in B is shown as a filled rectangle. The *Bgl*II fragment detected in the wild-type allele does not have a *Hha*I site. Gray bars below each map (VIII and VIII′) indicate regions analyzed by bisulfite sequencing in C, D and E. B, *Bam*HI; Sa, *Sac*I sites; dots 1-4, CTCF binding sites. (B) DNA methylation status of the paternally inherited mutant (5′ICR-KO) allele in tail somatic cells. Tail DNA of mutant mice (WT/KO^{pat}) was digested with *Bgl*II and then *Hha*I, and the blot was hybridized with the ICR-Ex probe. Asterisks indicate the positions of parental or methylated, undigested fragments. (C) DNA methylation status of the paternally inherited wild-type (region VIII′) or 5′ICR-KO (region VIII) *H19* ICR in somatic cells. Tail DNA was pooled, digested with *Xba*I, and treated with sodium bisulfite. Each region was amplified by PCR, subcloned, and sequenced. The numbers above each panel in the 5′ICR-KO results are the ID numbers of pooled samples (in B). The position of the *Hha*I sites in region VIII are shown by arrowheads. (D) DNA methylation status of the 5′ICR-KO allele (region VIII) in sperm from 7 mutant males was analyzed by bisulfite sequencing. (E) DNA methylation status of the paternally inherited 5′ICR-KO allele (region VIII) in 1-cell, 2-cell, and blastocyst stage embryos was analyzed by bisulfite sequencing. 22-33 (1-cell stage), 23-47 (2-cell stage), and 4-12 (blastocyst stage) embryos per agarose bead were used.

by the DNMT complex. In support of this notion, it has been recently reported that several maternal ICRs (*PLAGL1*, *INPP5F_v2*, and *PEG3*) in the macaque appeared to acquire allele-specific methylation only after fertilization (Cheong et al., 2015).

The paternally inherited hypomethylated transgenic *H19* ICR in two-cell embryos lacking the maternally supplied DNMT3L (Fig. 1E, Fig. S2A) was not capable of acquiring allele-specific methylation even after the implantation period (Fig. 1G), during which DNMT3L was zygotically expressed (Fig. S2A) (Guenatri et al., 2013; Hu et al., 2008). These results imply that the paternally inherited transgenic *H19* ICR must be recognized by the maternally supplied DNMT complex immediately after fertilization so that it is methylated during early embryogenesis. It is possible that *trans*-acting factors recruiting the DNMT complex to the epigenetically

Development (2015) 142, 3833-3844 doi:10.1242/dev.126003

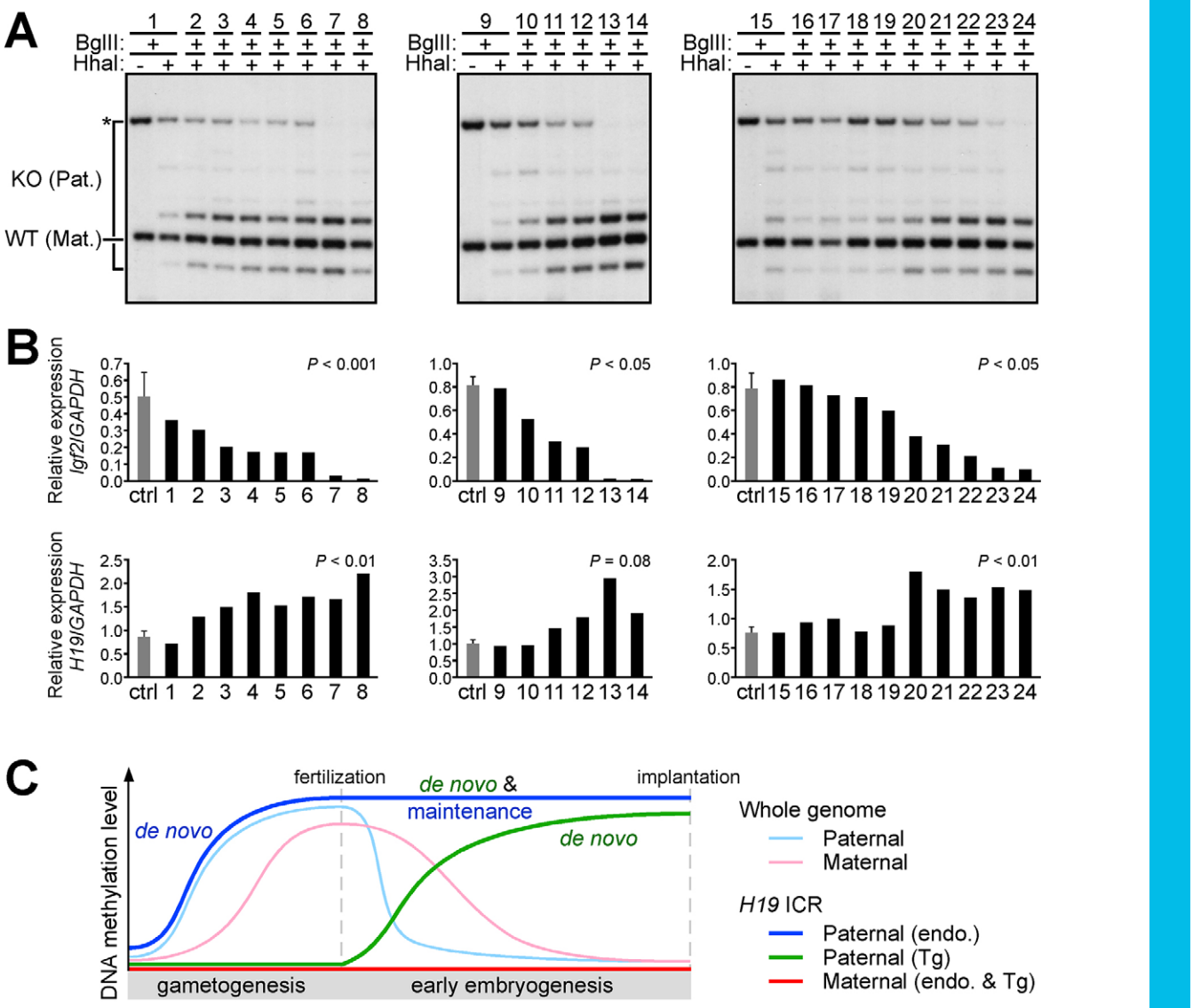

Fig. 7. *In vivo* role of the 5′-region of the endogenous *H19* ICR. (A) DNA methylation status of the paternally inherited mutant (5′ICR-KO) allele in the fetal liver. E12.5 embryos were obtained by mating wild-type females and hetero-KO males. The liver DNA of hetero-KO embryos (WT/KO^{pat}) was extracted and analyzed by Southern blotting as described above. Each panel shows the results of embryos from a single litter. Samples are arranged in order of their *Igf2* gene expression levels determined in B. (B) Expression levels of *Igf2* and *H19* in fetal livers. Total RNA was extracted from the livers of hetero-KO embryos (WT/KO^{pat}) and control (ctrl, WT/WT) littermates. The numbers correspond to those in A. The mRNA levels of *Igf2* (top) and *H19* (bottom) were measured by quantitative reverse transcription-PCR. Each value represents the ratio of *Igf2* or *H19* expression to that of *GAPDH*. For control embryos (sample numbers are 5, 8, and 5 in each litter: from left to right), the mean±s.d. is shown. The differences in the means between control and KO embryos were tested using an unpaired *t*-test. (C) A model of postfertlization maintenance of methylation imprint at the *H19* ICR. During early embryogenesis, mammalian genomes undergo extensive epigenetic reprogramming, such as genome-wide DNA demethylation. Even in this environment, the allelic DNA methylation of ICRs is faithfully maintained at the imprinted loci, suggesting their states are selectively protected. Based on our observations, we propose that the postfertilization, *de novo* DNA methylation activity of the *H19* ICR contributes to maintain its imprint in early embryos.

marked paternal *H19* ICR might be present only during this short period after fertilization. Alternatively, the hypothetical allele-specific epigenetic mark on the *H19* ICR itself might be lost as embryonic development proceeds.

Possible candidates for the epigenetic signatures marked during spermatogenesis are histone modifications and/or association with specific histone variants. In sperm, 1% and 15% of the genomes are associated with histones rather than protamines in mice and humans, respectively (Miller et al., 2010), and importantly, imprinted loci including the *Igf2/H19* locus are among those regions (Hammoud et al., 2009). We reported that, in sperm, H3K9me2 is preferentially enriched at the paternally methylated endogenous ICRs (e.g. *H19* and *Rasgrf1* ICRs) (Nakamura et al., 2012). Therefore, histone modification or histone variants within the transgenic *H19* ICR might be transmitted to zygotes to attract the DNMT complex to introduce DNA methylation.

Methylation acquisition at the endogenous *H19* ICR that is flanked by cHS4c sequences was partially obstructed in sperm (Fig. 2B, Fig. S4B). After fertilization, its methylation level was moderately recovered (Fig. 2C, Fig. 3C, Fig. S4C,E), and maternally provided DNMT3L played a significant role in this process (Fig. 3). Therefore, similar to the transgenic *H19* ICR, the endogenous *H19* ICR likely acquired an unknown epigenetic mark during spermatogenesis, and after fertilization, the *de novo*

Development (2015) 142, 3833-3844 doi:10.1242/dev.126003

DNA methylation machinery recognized the mark for allele discrimination. If a common epigenomic state can be identified in the DNA-methylated endogenous *H19* ICR and unmethylated transgenic *H19* ICR sequences in sperm, that would constitute a strong candidate for the primary mark that instructs imprinted DNA methylation in early embryos, because the mark cannot be secondary to DNA methylation.

Although some maternally methylated ICRs (*Snrpn* and *Peg3*) have been suggested to acquire allele-specific methylation after fertilization in mouse, these cases were not maternal DNMT3L dependent (Arnaud et al., 2006; Henckel et al., 2009). Therefore, the mechanistic basis of postfertilization methylation in the *H19* and other ICRs might be distinct. Additionally, as far as we know our data also provide the first example demonstrating a role for DNMT3L during early embryogenesis.

We have previously proposed that, in early embryos, Stella was involved in the maintenance of the hypermethylation status of the endogenous *H19* ICR, by inhibiting Tet3-mediated conversion of 5-methylcytosine to 5-hydroxymethylcytosine (Nakamura et al., 2012). We therefore tested whether the methylation status of the transgenic *H19* ICR, established *de novo* by DNMT3A and DNMT3L was also protected by this molecule. Maternal deletion of the *Stella* gene in oocytes caused a partial loss of methylation at the paternally inherited transgenic *H19* ICR in two-cell embryos (Fig. S1G). It was therefore suggested that Stella plays a shared role in the endogenous and transgenic *H19* ICR.

To demonstrate a role for postfertilization paternal allele-specific methylation activity at the endogenous locus, we narrowed its essential sequences in YAC-TgM (Figs 4 and 5) (Okamura et al., 2013b) and deleted them from the endogenous paternal *H19* ICR. Although gametic methylation of the mutant, endogenous *H19* ICR was not affected, its methylation level was diminished soon after fertilization (Fig. 6), demonstrating that the deleted region contains *cis* elements required for maintaining allele-specific methylation levels during early embryogenesis. A DNA-binding protein complex recognizing this region might interact with the *de novo* DNMT complex or with factors involved in the regulation of the DNA methylation status of the *H19* ICR. Another possibility is that an epigenetic mark to designate its paternal origin might be set in this region of the *H19* ICR during spermatogenesis. Importantly, this is the first example of regulatory sequences that ensure a stable methylation level of the paternal *H19* ICR during preimplantation periods, because all the *cis* regulatory elements identified to date (such as CTCF or Sox-Oct binding motifs) function to maintain the unmethylated state of maternal *H19* ICR following implantation (Matsuzaki et al., 2010; Sakaguchi et al., 2013; Schoenherr et al., 2003; Zimmerman et al., 2013).

Paternal inheritance of the 5′ICR-KO allele resulted in its partial loss of DNA methylation (Fig. 7A), decreased and increased expression of *Igf2* and *H19*, respectively (Fig. 7B), and reduced body weight of the mutant embryos (Fig. S8). Because we observed partial penetrance of these phenotypes, we repeated these experiments after backcrossing the mutant mice onto C57BL/6 for five generations after which essentially the same results were obtained (data not shown). Therefore, any phenotypic variability among embryos is not attributable to genetic background. Some part of maintenance and/or *de novo* methylation machinery in early embryos might have a stochastic nature and contribute to generation of such variations.

In summary, we delineated the postfertilization allele-specific *de novo* DNA methylation activity in the transgenic *H19* ICR and identified its 5′-region as an essential element for this activity. Deletion of this element from the endogenous mouse *H19* ICR resulted in a loss of methylation on the paternal allele, dysregulation of both *Igf2* and *H19* expression, and growth retardation. We propose that the activity we uncovered plays a role in maintaining allele-specific methylation at the endogenous *H19* ICR in preimplantation embryos, and that the *de novo* methylation imprinting activity at the *H19* ICR and genome-wide demethylation activity are in a state of dynamic equilibrium during this period (Fig. 7C).

MATERIALS AND METHODS

Mice

Transgenic mice carrying a human β-globin YAC, in which the 2.9-kb *H19* ICR fragment was inserted between the LCR and the ε-globin gene were described previously (Tanimoto et al., 2005). *Dnmt3l* KO mice were kindly provided by Dr En Li (Hata et al., 2002). *Dnmt3a-2lox* (RBRC03731) (Kaneda et al., 2004) and *Dnmt3b-2lox* (RBRC03733) (Dodge et al., 2005) mice were generous gifts from Dr Masaki Okano and provided by RIKEN BRC through the National Bio-Resource Project of the Ministry of Education, Culture, Sports, Science and Technology (MEXT), Japan. To conditionally disrupt the floxed alleles in oocytes, these mice were crossed with TgM carrying *Zp3-Cre* gene (Jackson Laboratory; de Vries et al., 2000). Insulated *H19* ICR knock-in mice, ICR4321S TgM, ICR432 TgM, and 5′ICR KO mice were generated as described in the supplementary materials and methods.

Animal experiments were performed in a humane manner and approved by the Institutional Animal Experiment Committee of the University of Tsukuba. Experiments were conducted in accordance with the Regulation of Animal Experiments of the University of Tsukuba and the Fundamental Guidelines for Proper Conduct of Animal Experiments and Related Activities in Academic Research Institutions under the jurisdiction of the MEXT.

Preparation of oocytes and embryos

Female mice were super-ovulated via injection of pregnant mare serum gonadotropin, followed by human chorionic gonadotropin (hCG) (47-48 h interval). Unfertilized oocytes were collected from oviducts 18 h after hCG injection, and cumulus cells were removed by hyaluronidase treatment. Fertilized one-cell zygotes were collected from mated females 24 h after hCG injection, and cumulus cells were removed. Two- and eight-cell embryos were flushed from oviducts at 44 and 68 h, respectively, after hCG injection. Embryos at E3.5 (blastocysts), E8.5, and E12.5 were obtained by natural mating.

DNA methylation analysis by bisulfite sequencing

Preimplantation embryos were embedded in agarose beads and treated with sodium bisulfite as described previously (Matsuzaki et al., 2009). Genomic DNA extracted from postimplantation embryos (E8.5), adult male sperm, or the tail tips of ∼1-week-old animals was treated with sodium bisulfite using the EZ DNA Methylation Kit (Zymo Research). Sperm and tail tip DNA was digested with *Xba*I prior to the treatment. Subregions of the *H19* ICR in transgenic and knock-in/KO mice were amplified by nested and single-round PCR, respectively, and the fragments were subcloned into the pGEM-T Easy vector (Promega) for sequencing analyses. PCR primers are listed in Tables S1, S2. Nested PCR was employed to distinguish between the endogenous and transgenic *H19* ICR sequences.

DNA methylation analysis by Southern blotting

Genomic DNA from ICR4321S TgM and 5′ICR-KO mice were first digested by *Eco*T22I and *Bgl*II, respectively, to liberate the *H19* ICR region and subjected to the methylation-sensitive enzymes *Bst*UI and *Hha*I, respectively. Following size separation in agarose gels, Southern blots were hybridized with α-^{32}P-labeled probes and subjected to X-ray film autoradiography.

RT-qPCR

Total RNA of the liver at E12.5 was extracted by ISOGEN (Nippon Gene) and converted to cDNA using ReverTra Ace qPCR RT Master Mix with

Development (2015) 142, 3833-3844 doi:10.1242/dev.126003

gDNA Remover (TOYOBO). Quantitative amplification of cDNA was performed with the Thermal Cycler Dice (TaKaRa Bio) using SYBR Premix EX TaqII (TaKaRa Bio) and PCR primers listed in Table S3.

Acknowledgements

We thank Drs Doug Engel (University of Michigan) and Jörg Bungert (University of Florida) for critically reading the manuscript.

Competing interests

The authors declare no competing or financial interests.

Author contributions

H.M., E.O. and K.T. designed the experiments. H.M., E.O., T.T., A.U. and K.T. performed the experiments. H.M., E.O., T.T. and K.T. analyzed the data. T. Nakamura, T. Nakano, K.H. and A.F. provided scientific advice and materials. H.M., E.O. and K.T. wrote the manuscript.

Funding

This work was supported in part by research grants from The Nakajima Foundation (to H.M.); The Kurata Memorial Hitachi Science and Technology Foundation (to H.M.); The Uehara Memorial Foundation (to K.T.); JSPS (Japan Society for the Promotion of Science) KAKENHI [26840113 Grant-in-Aid for Young Scientists (B) to H.M. and 26292189 Grant-in-Aid for Scientific Research (B) to K.T.]; and MEXT (Ministry of Education, Culture, Sports, Science and Technology) KAKENHI [26112503 Grant-in-Aid for Scientific Research on Innovative Areas to K.T.].

Supplementary information

Supplementary information available online at
http://dev.biologists.org/lookup/suppl/doi:10.1242/dev.126003/-/DC1

References

Arnaud, P., Hata, K., Kaneda, M., Li, E., Sasaki, H., Feil, R. and Kelsey, G. (2006). Stochastic imprinting in the progeny of Dnmt3L$^{-/-}$ females. *Hum. Mol. Genet.* **15**, 589-598.

Bell, A. C. and Felsenfeld, G. (2000). Methylation of a CTCF-dependent boundary controls imprinted expression of the Igf2 gene. *Nature* **405**, 482-485.

Cheong, C. Y., Chng, K., Ng, S., Chew, S. B., Chan, L. and Ferguson-Smith, A. C. (2015). Germline and somatic imprinting in the nonhuman primate highlights species differences in oocyte methylation. *Genome Res.* **25**, 611-623.

de Vries, W. N., Binns, L. T., Fancher, K. S., Dean, J., Moore, R., Kemler, R. and Knowles, B. B. (2000). Expression of Cre recombinase in mouse oocytes: a means to study maternal effect genes. *Genesis* **26**, 110-112.

DeChiara, T. M., Robertson, E. J. and Efstratiadis, A. (1991). Parental imprinting of the mouse insulin-like growth factor II gene. *Cell* **64**, 849-859.

Dickson, J., Gowher, H., Strogantsev, R., Gaszner, M., Hair, A., Felsenfeld, G. and West, A. G. (2010). VEZF1 elements mediate protection from DNA methylation. *PLoS Genet.* **6**, e1000804.

Dodge, J. E., Okano, M., Dick, F., Tsujimoto, N., Chen, T., Wang, S., Ueda, Y., Dyson, N. and Li, E. (2005). Inactivation of Dnmt3b in mouse embryonic fibroblasts results in DNA hypomethylation, chromosomal instability, and spontaneous immortalization. *J. Biol. Chem.* **280**, 17986-17991.

Ferguson-Smith, A. C. (2011). Genomic imprinting: the emergence of an epigenetic paradigm. *Nat. Rev. Genet.* **12**, 565-575.

Gabory, A., Jammes, H. and Dandolo, L. (2010). The H19 locus: role of an imprinted non-coding RNA in growth and development. *Bioessays* **32**, 473-480.

Gebert, C., Kunkel, D., Grinberg, A. and Pfeifer, K. (2010). H19 imprinting control region methylation requires an imprinted environment only in the male germ line. *Mol. Cell. Biol.* **30**, 1108-1115.

Guenatri, M., Duffie, R., Iranzo, J., Fauque, P. and Bourc'his, D. (2013). Plasticity in Dnmt3L-dependent and -independent modes of de novo methylation in the developing mouse embryo. *Development* **140**, 562-572.

Hammoud, S. S., Nix, D. A., Zhang, H., Purwar, J., Carrell, D. T. and Cairns, B. R. (2009). Distinctive chromatin in human sperm packages genes for embryo development. *Nature* **460**, 473-478.

Hark, A. T., Schoenherr, C. J., Katz, D. J., Ingram, R. S., Levorse, J. M. and Tilghman, S. M. (2000). CTCF mediates methylation-sensitive enhancer-blocking activity at the H19/Igf2 locus. *Nature* **405**, 486-489.

Hata, K., Okano, M., Lei, H. and Li, E. (2002). Dnmt3L cooperates with the Dnmt3 family of de novo DNA methyltransferases to establish maternal imprints in mice. *Development* **129**, 1983-1993.

Henckel, A., Nakabayashi, K., Sanz, L. A., Feil, R., Hata, K. and Arnaud, P. (2009). Histone methylation is mechanistically linked to DNA methylation at imprinting control regions in mammals. *Hum. Mol. Genet.* **18**, 3375-3383.

Henckel, A., Chebli, K., Kota, S. K., Arnaud, P. and Feil, R. (2012). Transcription and histone methylation changes correlate with imprint acquisition in male germ cells. *EMBO J.* **31**, 606-615.

Hirasawa, R., Chiba, H., Kaneda, M., Tajima, S., Li, E., Jaenisch, R. and Sasaki, H. (2008). Maternal and zygotic Dnmt1 are necessary and sufficient for the maintenance of DNA methylation imprints during preimplantation development. *Genes Dev.* **22**, 1607-1616.

Hu, Y.-G., Hirasawa, R., Hu, J.-L., Hata, K., Li, C.-L., Jin, Y., Chen, T., Li, E., Rigolet, M., Viegas-Pequignot, E. et al. (2008). Regulation of DNA methylation activity through Dnmt3L promoter methylation by Dnmt3 enzymes in embryonic development. *Hum. Mol. Genet.* **17**, 2654-2664.

Kaneda, M., Okano, M., Hata, K., Sado, T., Tsujimoto, N., Li, E. and Sasaki, H. (2004). Essential role for de novo DNA methyltransferase Dnmt3a in paternal and maternal imprinting. *Nature* **429**, 900-903.

Kelsey, G. and Feil, R. (2013). New insights into establishment and maintenance of DNA methylation imprints in mammals. *Philos. Trans. R. Soc. B Biol. Sci.* **368**, 20110336.

Kobayashi, H., Sakurai, T., Imai, M., Takahashi, N., Fukuda, A., Yayoi, O., Sato, S., Nakabayashi, K., Hata, K., Sotomaru, Y. et al. (2012). Contribution of intragenic DNA methylation in mouse gametic DNA methylomes to establish oocyte-specific heritable marks. *PLoS Genet.* **8**, e1002440.

Li, X., Ito, M., Zhou, F., Youngson, N., Zuo, X., Leder, P. and Ferguson-Smith, A. C. (2008). A maternal-zygotic effect gene, Zfp57, maintains both maternal and paternal imprints. *Dev. Cell* **15**, 547-557.

Ma, P., Lin, S., Bartolomei, M. S. and Schultz, R. M. (2010). Metastasis tumor antigen 2 (MTA2) is involved in proper imprinted expression of H19 and Peg3 during mouse preimplantation development. *Biol. Reprod.* **83**, 1027-1035.

Matsuzaki, H., Okamura, E., Shimotsuma, M., Fukamizu, A. and Tanimoto, K. (2009). A randomly integrated transgenic H19 imprinting control region acquires methylation imprinting independently of its establishment in germ cells. *Mol. Cell. Biol.* **29**, 4595-4603.

Matsuzaki, H., Okamura, E., Fukamizu, A. and Tanimoto, K. (2010). CTCF binding is not the epigenetic mark that establishes post-fertilization methylation imprinting in the transgenic H19 ICR. *Hum. Mol. Genet.* **19**, 1190-1198.

Messerschmidt, D. M., de Vries, W., Ito, M., Solter, D., Ferguson-Smith, A. and Knowles, B. B. (2012). Trim28 is required for epigenetic stability during mouse oocyte to embryo transition. *Science* **335**, 1499-1502.

Miller, D., Brinkworth, M. and Iles, D. (2010). Paternal DNA packaging in spermatozoa: more than the sum of its parts? DNA, histones, protamines and epigenetics. *Reproduction* **139**, 287-301.

Nakamura, T., Arai, Y., Umehara, H., Masuhara, M., Kimura, T., Taniguchi, H., Sekimoto, T., Ikawa, M., Yoneda, Y., Okabe, M. et al. (2007). PGC7/Stella protects against DNA demethylation in early embryogenesis. *Nat. Cell Biol.* **9**, 64-71.

Nakamura, T., Liu, Y.-J., Nakashima, H., Umehara, H., Inoue, K., Matoba, S., Tachibana, M., Ogura, A., Shinkai, Y. and Nakano, T. (2012). PGC7 binds histone H3K9me2 to protect against conversion of 5mC to 5hmC in early embryos. *Nature* **486**, 415-419.

Okamura, E., Matsuzaki, H., Fukamizu, A. and Tanimoto, K. (2013a). The chicken HS4 insulator element does not protect the H19 ICR from differential DNA methylation in yeast artificial chromosome transgenic mouse. *PLoS ONE* **8**, e73925.

Okamura, E., Matsuzaki, H., Sakaguchi, R., Takahashi, T., Fukamizu, A. and Tanimoto, K. (2013b). The H19 imprinting control region mediates preimplantation imprinted methylation of nearby sequences in yeast artificial chromosome transgenic mice. *Mol. Cell. Biol.* **33**, 858-871.

Okano, M., Bell, D. W., Haber, D. A. and Li, E. (1999). DNA methyltransferases Dnmt3a and Dnmt3b are essential for de novo methylation and mammalian development. *Cell* **99**, 247-257.

Park, K.-Y., Sellars, E. A., Grinberg, A., Huang, S.-P. and Pfeifer, K. (2004). The H19 differentially methylated region marks the parental origin of a heterologous locus without gametic DNA methylation. *Mol. Cell. Biol.* **24**, 3588-3595.

Puget, N., Hirasawa, R., Hu, N.-S. N., Laviolette-Malirat, N., Feil, R. and Khamlichi, A. A. (2015). Insertion of an imprinted insulator into the IgH locus reveals developmentally regulated, transcription-dependent control of V(D)J recombination. *Mol. Cell. Biol.* **35**, 529-543.

Quenneville, S., Verde, G., Corsinotti, A., Kapopoulou, A., Jakobsson, J., Offner, S., Baglivo, I., Pedone, P. V., Grimaldi, G., Riccio, A. et al. (2011). In embryonic stem cells, ZFP57/KAP1 recognize a methylated hexanucleotide to affect chromatin and DNA methylation of imprinting control regions. *Mol. Cell* **44**, 361-372.

Reese, K. J., Lin, S., Verona, R. I., Schultz, R. M. and Bartolomei, M. S. (2007). Maintenance of paternal methylation and repression of the imprinted H19 gene requires MBD3. *PLoS Genet.* **3**, e137.

Sakaguchi, R., Okamura, E., Matsuzaki, H., Fukamizu, A. and Tanimoto, K. (2013). Sox-Oct motifs contribute to maintenance of the unmethylated H19 ICR in YAC transgenic mice. *Hum. Mol. Genet.* **22**, 4627-4637.

Schoenherr, C. J., Levorse, J. M. and Tilghman, S. M. (2003). CTCF maintains differential methylation at the Igf2/H19 locus. *Nat. Genet.* **33**, 66-69.

Development (2015) 142, 3833-3844 doi:10.1242/dev.126003

Smallwood, S. A., Tomizawa, S.-i., Krueger, F., Ruf, N., Carli, N., Segonds-Pichon, A., Sato, S., Hata, K., Andrews, S. R. and Kelsey, G. (2011). Dynamic CpG island methylation landscape in oocytes and preimplantation embryos. *Nat. Genet.* **43**, 811-814.

Srivastava, M., Hsieh, S., Grinberg, A., Williams-Simons, L., Huang, S. P. and Pfeifer, K. (2000). H19 and Igf2 monoallelic expression is regulated in two distinct ways by a shared cis acting regulatory region upstream of H19. *Genes Dev.* **14**, 1186-1195.

Szabo, P. E., Tang, S. H., Reed, M. R., Silva, F. J., Tsark, W. M. and Mann, J. R. (2002). The chicken beta-globin insulator element conveys chromatin boundary activity but not imprinting at the mouse Igf2/H19 domain. *Development* **129**, 897-904.

Tanimoto, K., Shimotsuma, M., Matsuzaki, H., Omori, A., Bungert, J., Engel, J. D. and Fukamizu, A. (2005). Genomic imprinting recapitulated in the human beta-globin locus. *Proc. Natl. Acad. Sci. USA* **102**, 10250-10255.

Tanimoto, K., Sugiura, A., Kanafusa, S., Saito, T., Masui, N., Yanai, K. and Fukamizu, A. (2008). A single nucleotide mutation in the mouse renin promoter disrupts blood pressure regulation. *J. Clin. Invest.* **118**, 1006-1016.

Tomizawa, S.-i. and Sasaki, H. (2012). Genomic imprinting and its relevance to congenital disease, infertility, molar pregnancy and induced pluripotent stem cell. *J. Hum. Genet.* **57**, 84-91.

Tremblay, K. D., Duran, K. L. and Bartolomei, M. S. (1997). A 5′ 2-kilobase-pair region of the imprinted mouse H19 gene exhibits exclusive paternal methylation throughout development. *Mol. Cell. Biol.* **17**, 4322-4329.

West, A. G., Huang, S., Gaszner, M., Litt, M. D. and Felsenfeld, G. (2004). Recruitment of histone modifications by USF proteins at a vertebrate barrier element. *Mol. Cell* **16**, 453-463.

Zimmerman, D. L., Boddy, C. S. and Schoenherr, C. S. (2013). Oct4/Sox2 binding sites contribute to maintaining hypomethylation of the maternal igf2/h19 imprinting control region. *PLoS ONE* **8**, e81962.

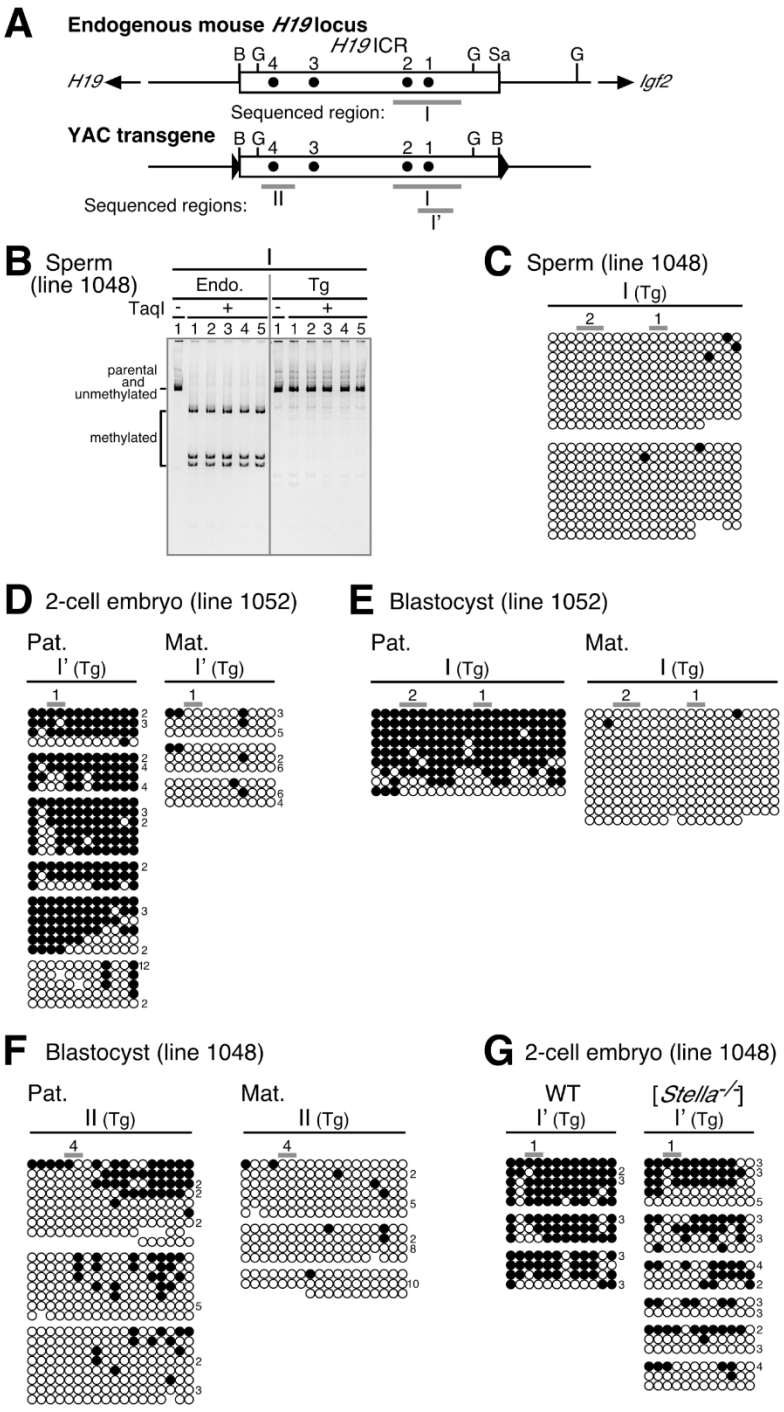

Fig. S1. DNA methylation status of the transgenic *H19* imprinting control region (ICR) in sperm and early embryos

(A) Structure of the *H19* ICR in the endogenous (upper) and ICR/β-globin yeast artificial chromosome transgene (YAC, lower) loci. Region I (endogenous) or regions I, I', and II (transgenic) of the *H19* ICR, indicated by gray bars, were analyzed by COBRA (B) or bisulfite sequencing (C-G). Sa; *Sac*I, B; *Bam*HI, G; *Bgl*II sites.

(B) Sperm was obtained from the cauda epididymis of male ICR/β-globin YAC-transgenic mice (TgM) (line 1048). Genomic DNA was extracted and treated with sodium bisulfite. The endogenous or transgenic *H19* ICR regions [I shown in (A)] were amplified by nested PCR using locus-specific primers for first-round PCR. The aliquots of PCR products were digested with *Taq*I (+) to assess the methylation status of the original DNA.

(C) The methylation status of the transgenic *H19* ICR region I in sperm (line 1048) was analyzed by bisulfite sequencing. Each horizontal row represents a single DNA template molecule. Methylated and unmethylated CpG motifs are indicated by filled and open circles, respectively.

(D) The methylation status of the transgenic *H19* ICR region I' in 2-cell embryos (11–48 embryos) that inherited YAC transgene (line 1052) paternally (Pat.) or maternally (Mat.) was analyzed by bisulfite sequencing.

(E, F) The methylation status of the transgenic *H19* ICR regions I (E; line 1052) or II (F; line 1048) in blastocysts (31 and 42 embryos in E, 4-12 embryos in F) that inherited the YAC transgene paternally (Pat.) or maternally (Mat.) was analyzed by bisulfite sequencing.

(G) A role of Stella in the post-fertilization methylation of the paternally inherited transgenic *H19* ICR. Two-cell stage embryos were obtained from wild-type (WT) or [*Stella*$^{-/-}$] females crossed with ICR/β-globin male TgM (line 1048, carrying the WT *Stella* gene) and embedded in agarose beads (6–13 embryos per beads were used). The methylation status of the paternally inherited transgenic *H19* ICR region I' was analyzed by bisulfite sequencing.

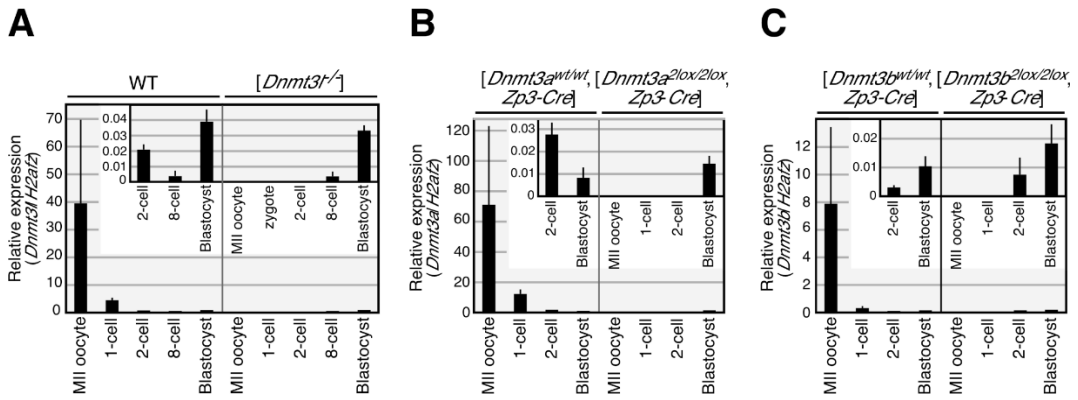

Fig. S2. Expression of *de novo* DNA methyltransferases in oocytes and preimplantation embryos

(A) [*Dnmt3l*$^{-/-}$], (B) [*Dnmt3a*$^{2lox/2lox}$, *Zp3-Cre*], and (C) [*Dnmt3b*$^{2lox/2lox}$, *Zp3-Cre*] females, as well as their corresponding controls ([*Dnmt3l*$^{+/+}$ (wild-type)], [*Dnmt3a*$^{wt/wt}$, *Zp3-Cre*], and [*Dnmt3b*$^{wt/wt}$, *Zp3-Cre*], respectively), were mated with wild-type males, and total RNA was isolated from their MII oocytes and embryos. The levels of *Dnmt3l* (A), *Dnmt3a* (B), or *Dnmt3b* (C) mRNA accumulation were measured by RT-qPCR. Each value represents the ratio of *Dnmt* expression to that of histone *H2afz*. Each sample was analyzed at least three times, and the means ± SD are shown.

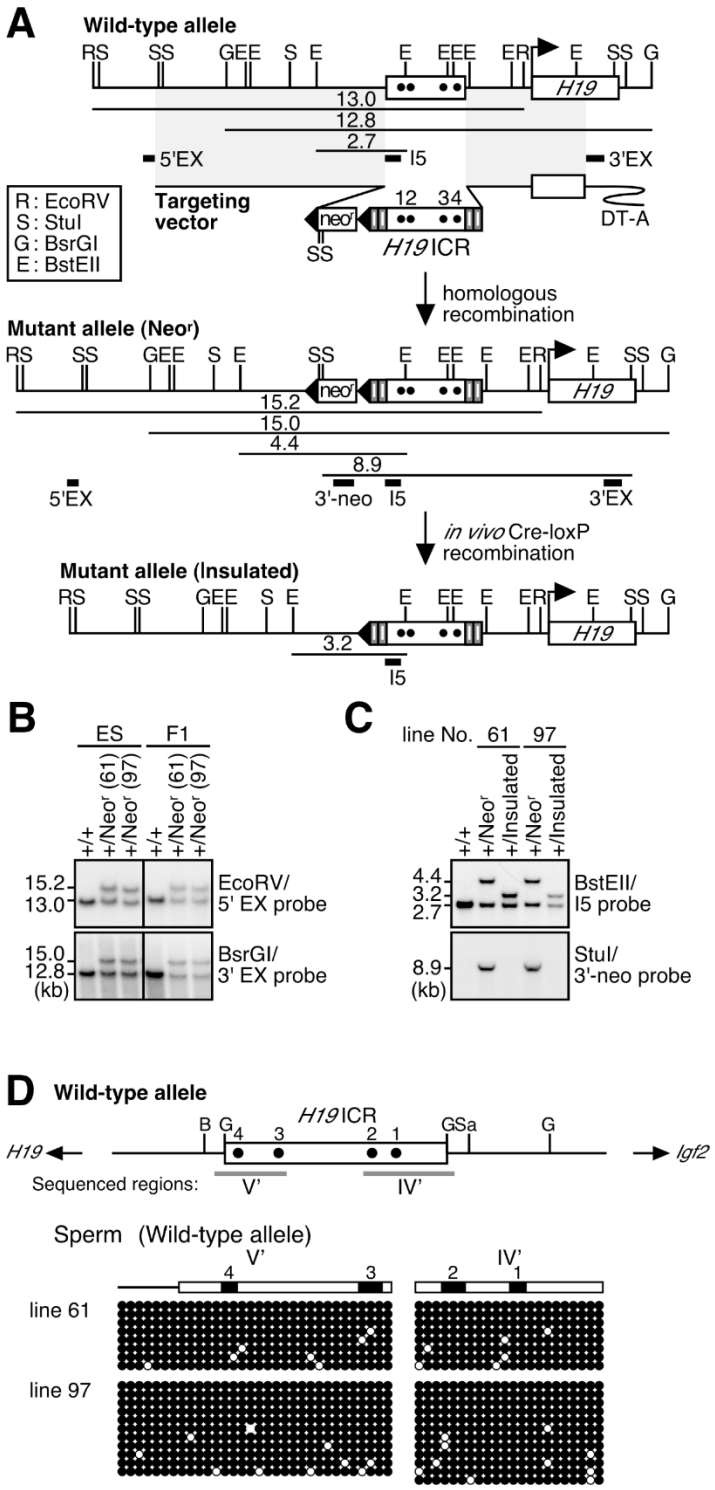

Fig. S3. Generation of insulated *H19* ICR knock-in mice

(A) Targeting strategy at the *H19* locus. Maps of the wild-type allele, the targeting vector with the *H19* ICR fragment flanked by tandemly arrayed cHS4c sequences (I for insulator, gray rectangles), the correctly targeted allele [Mutant allele (Neo^r)], and the targeted allele after Cre-mediated excision of the neo^r gene cassette [Mutant allele (Insulated)] are shown

from top to bottom. The solid triangles indicate the loxP sequences. Probes used for Southern blot analyses in (B) and (C) are shown as filled rectangles. The positions of restriction enzyme sites and expected restriction enzyme fragments with their sizes are shown beneath the each map.

(B) Genomic DNA from ES clones and mutant mouse tails was digested with *Eco*RV (top) or *Bsr*GI (bottom) and separated on agarose gels, and Southern blots were hybridized to the 5'EX or 3'EX probes, respectively.

(C) Tail genomic DNA of mutant mice, before (Neo^r) or after (Insulated) *in vivo* Cre-loxP recombination, was digested with *Bst*EII (top) or *Stu*I (bottom) and separated on agarose gels, and Southern blots were hybridized to the I5 or 3'-neo probes, respectively.

(D) (Top) Map of the wild-type *H19* gene locus. B; *Bam*HI, G; *Bgl*II, Sa; *Sac*I sites. Two regions (V' and IV') analyzed by bisulfite sequencing are shown as gray bars beneath the map. (Bottom) Genomic DNA extracted from the sperm of hetero-mutant mice (lines 61 and 97, which were analyzed in Fig. 2B) were digested with *Xba*I and treated with sodium bisulfite. Regions V' and IV' of the WT allele were amplified by PCR, subcloned, and sequenced.

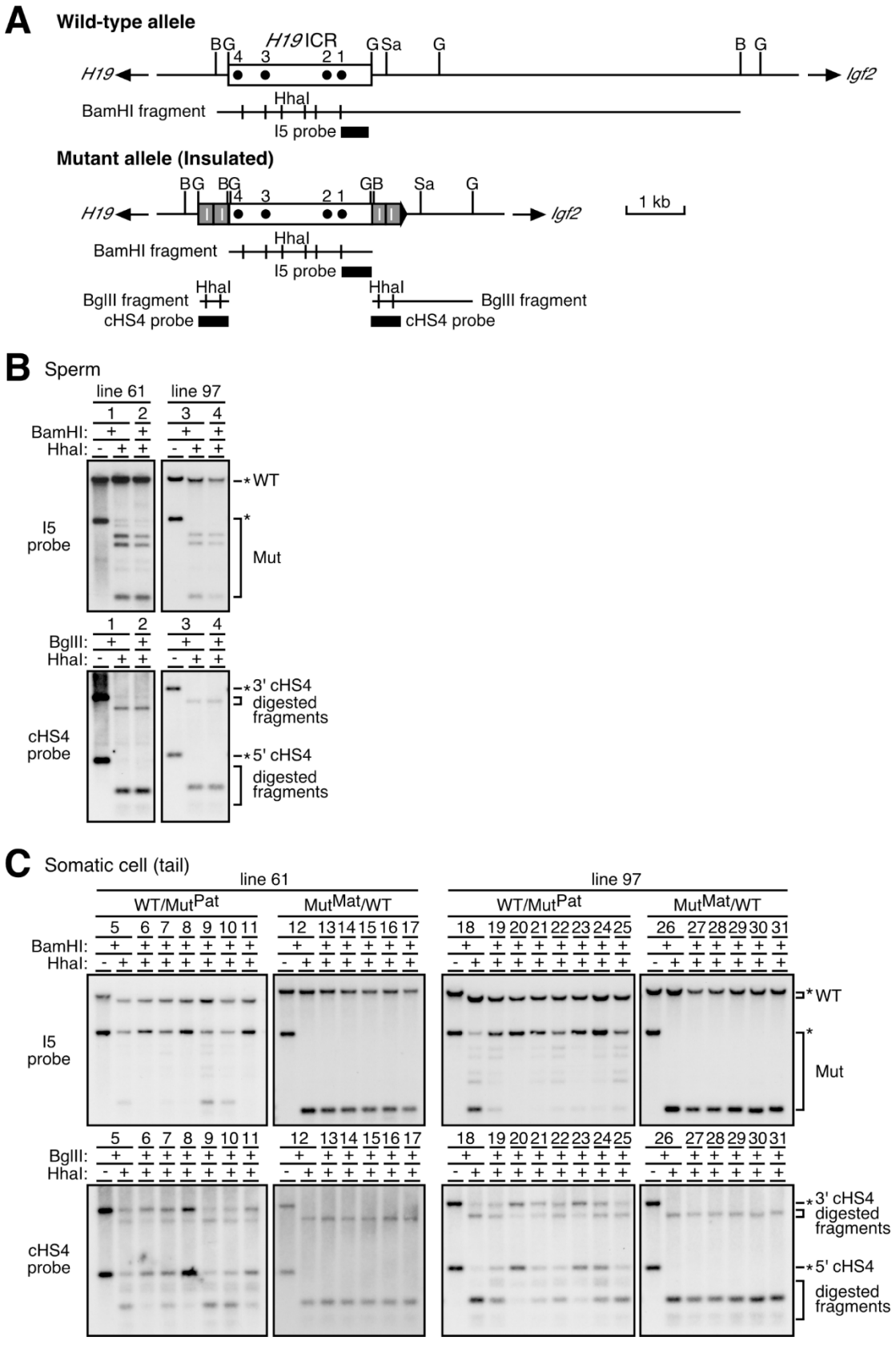

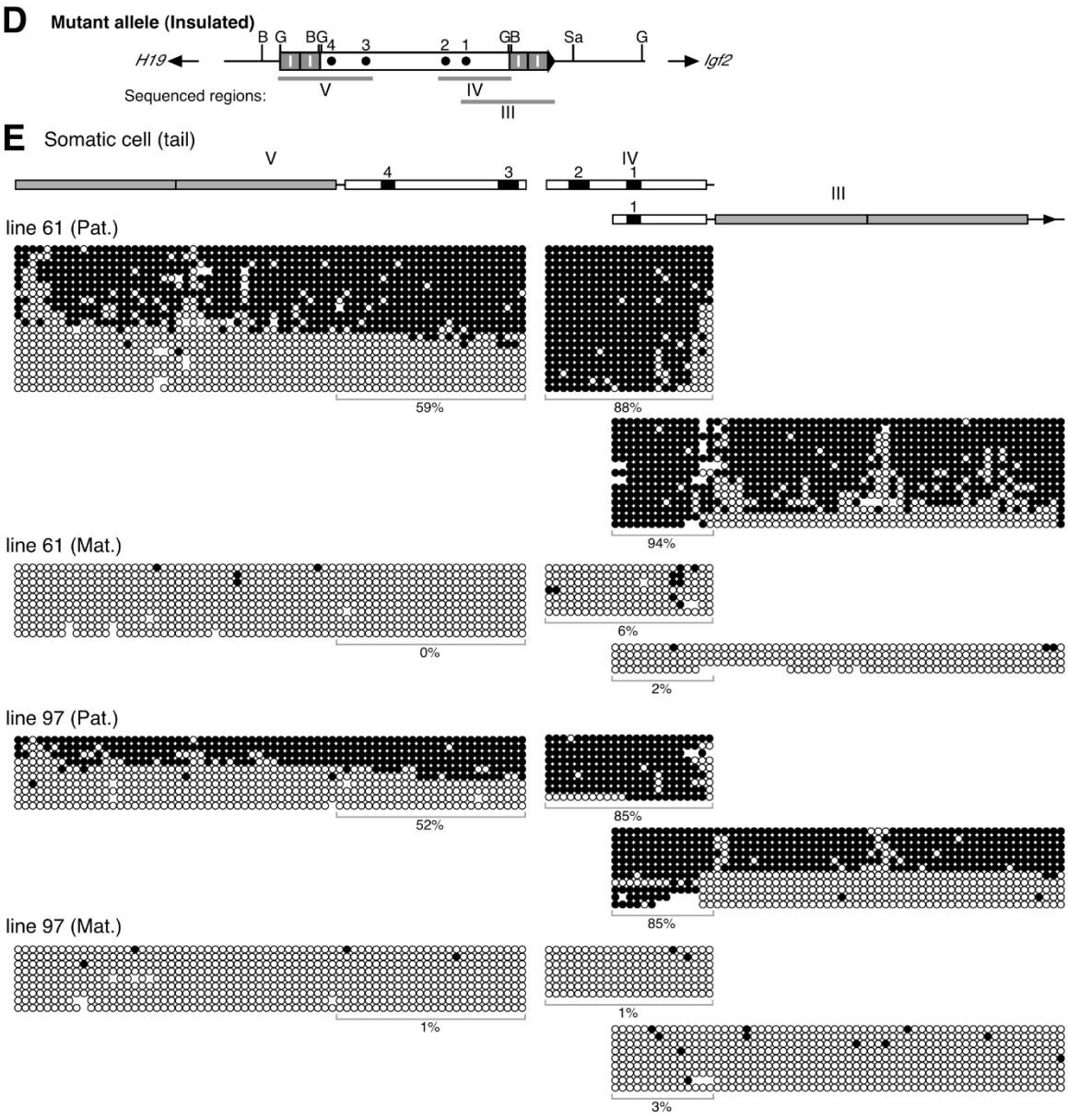

Fig. S4. DNA methylation status of the insulated *H19* ICR in sperm and somatic cells

(A) Partial restriction enzyme maps of the wild-type (WT) and mutant (insulated, Mut) *H19* loci. Methylation-sensitive *Hha*I sites in the *Bam*HI (B) and *Bgl*II (G) fragments are displayed as vertical lines beneath each map. Probes used for Southern blot analysis in

(B) and (C) are shown as filled rectangles. Sa; *Sac*I site.

(B, C) DNA methylation status of the *H19* ICR (top) and cHS4c (bottom) sequences in sperm (B) and somatic cells (neonatal tail tips) (C) of the mutant mice (lines 61 and 97) that inherited the mutant allele either paternally (WT/Mut^{Pat}) or maternally (Mut^{Mat}/WT). To analyze the *H19* ICR sequences, sperm or tail DNA was digested with *Bam*HI and then *Hha*I, and the blots were hybridized with the I5 probe shown in (A). To analyze the cHS4c sequences, DNA was digested with *Bgl*II and then *Hha*I, and the blots were hybridized with the cHS4 probe. WT; wild-type allele, Mut; mutant (insulated) allele. Asterisks indicate the positions of parental or methylated undigested fragments.

(D) Map of the mutant (insulated) *H19* locus. Three regions of the mutant allele (III, IV, and V) analyzed by bisulfite sequencing in (E) are shown as gray bars beneath the map. B; *Bam*HI, G; *Bgl*II, Sa; *Sac*I sites.

(E) Genomic DNA extracted from tail tips of neonates that inherited the mutant (insulated) allele either paternally (Pat.) or maternally (Mat.) (lines 61 and 97) were digested with *Xba*I and treated with sodium bisulfite. The three regions shown in (D) were amplified by PCR, subcloned, and sequenced. The overall percentage of methylated CpGs in region IV or those in the ICR portions of region III or V are indicated next to each panel.

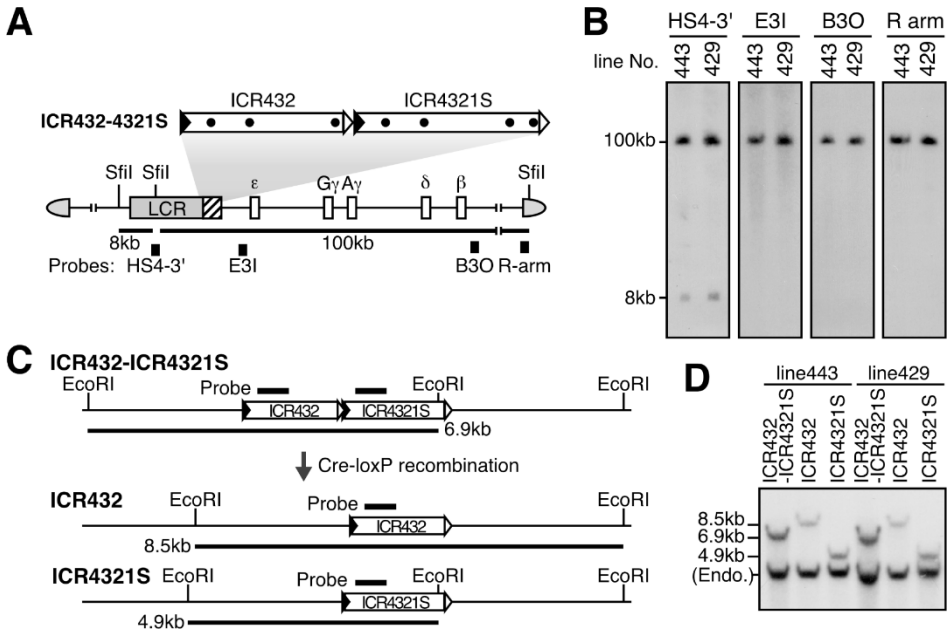

Fig. S5. Generation and structural analysis of YAC-TgM carrying the 5'-truncated *H19* ICR fragments

(A) Schematic representation of the YAC transgenes. The positions of the β-like globin genes (open boxes) are shown relative to the locus control region (LCR, gray box). *Sfi*I restriction enzyme sites are located 5' to the LCR, within the LCR, and in the right arm of the YAC. Probes (filled rectangles) used for long-range structural analyses shown in panels (B), and the expected restriction enzyme fragments and their sizes are shown. The enlarged map shows the detailed structure of the ICR432-ICR4321S fragments inserted between the LCR and the ε-globin gene. The positions of loxP5171 and loxP2272 are indicated as solid and open triangles, respectively.

(B) Long-range structural analysis of the transgenes in the ICR432-ICR4321S YAC-TgM. DNA from thymus cells was digested with *Sfi*I in agarose plugs and separated by pulsed-field gel electrophoresis, and Southern blots were hybridized separately to probes shown in (A).

(C) *In vivo* Cre-loxP recombination in the parental ICR432-ICR4321S transgene generates either ICR432 or ICR4321S daughter transgenes. Positions of *Eco*RI restriction enzyme sites, and the expected restriction enzyme fragments and their sizes are shown. For example, if recombination occurs between the loxP5171 sites (solid triangles), no further recombination can occur because one of the loxP2272 sites (open triangles) is concomitantly deleted. The probe used for Southern blot analysis in (D) was shown as filled rectangles.

(D) Tail DNA from each YAC-TgM sublines was digested with *Eco*RI and separated on agarose gels, and Southern blots were hybridized to the probe shown in (C). Endo.; fragments from the endogenous locus.

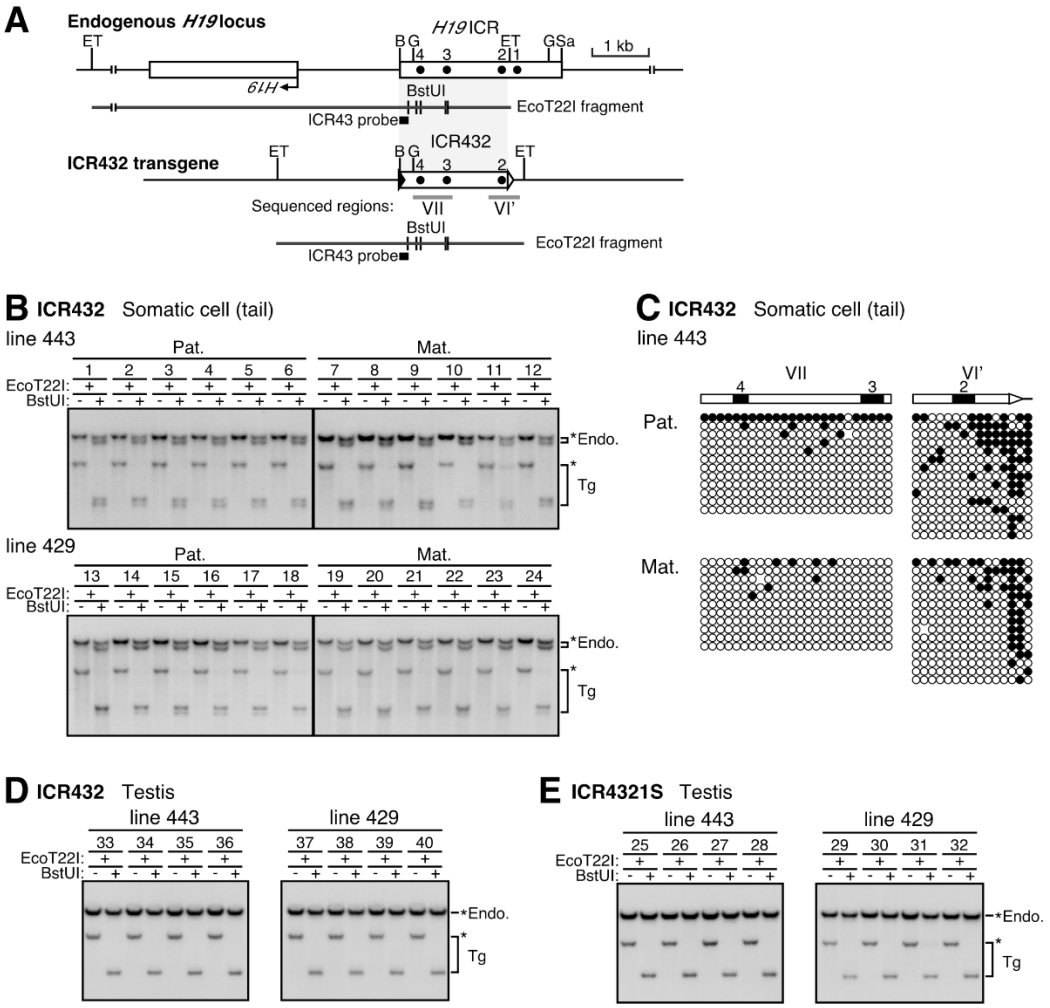

Fig. S6. DNA methylation status of the ICR432 and ICR4321S transgenes

(A) Partial restriction enzyme maps of the endogenous *H19* locus and the β-globin YAC transgene with the inserted ICR432 fragment. Methylation-sensitive *Bst*UI sites in the *Eco*T22I (ET) fragments are displayed as vertical lines beneath each map. The ICR43 probe used for Southern blot analysis in (B) and (D) is shown as a filled rectangle. B; *Bam*HI, G; *Bgl*II, Sa; *Sac*I sites. The two regions (VI' and VII) analyzed by bisulfite sequencing in (C) are shown as gray bars beneath the map.

(B) DNA methylation status of the ICR432 fragment in somatic cells of the YAC-TgM (lines 443 and 429) that inherited the transgenes either paternally (Pat.) or maternally (Mat.). Tail DNA was digested with *Eco*T22I and then *Bst*UI, and the blot was hybridized with the ICR43 probe shown in (A). Endo.; endogenous locus, Tg; transgene. Asterisks indicate the positions of parental or methylated, undigested fragments.

(C) DNA methylation status of regions VI' and VII [shown in (A)] in the somatic cells of the ICR432 YAC-TgM (line 443) that inherited the transgenes either paternally (Pat.) or maternally (Mat.). Tail DNA was digested with *Xba*I and treated with sodium bisulfite. The two regions were amplified by nested PCR, subcloned, and sequenced.

(D) DNA methylation status of the ICR432 fragment in testis of the YAC-TgM (lines 443 and 429). Testis DNA was analyzed by Southern blotting as described in (B).

(E) DNA methylation status of the ICR4321S fragment in testis of the YAC-TgM (lines 443 and 429). Testis DNA was analyzed by Southern blotting as described in Fig. 4C, D.

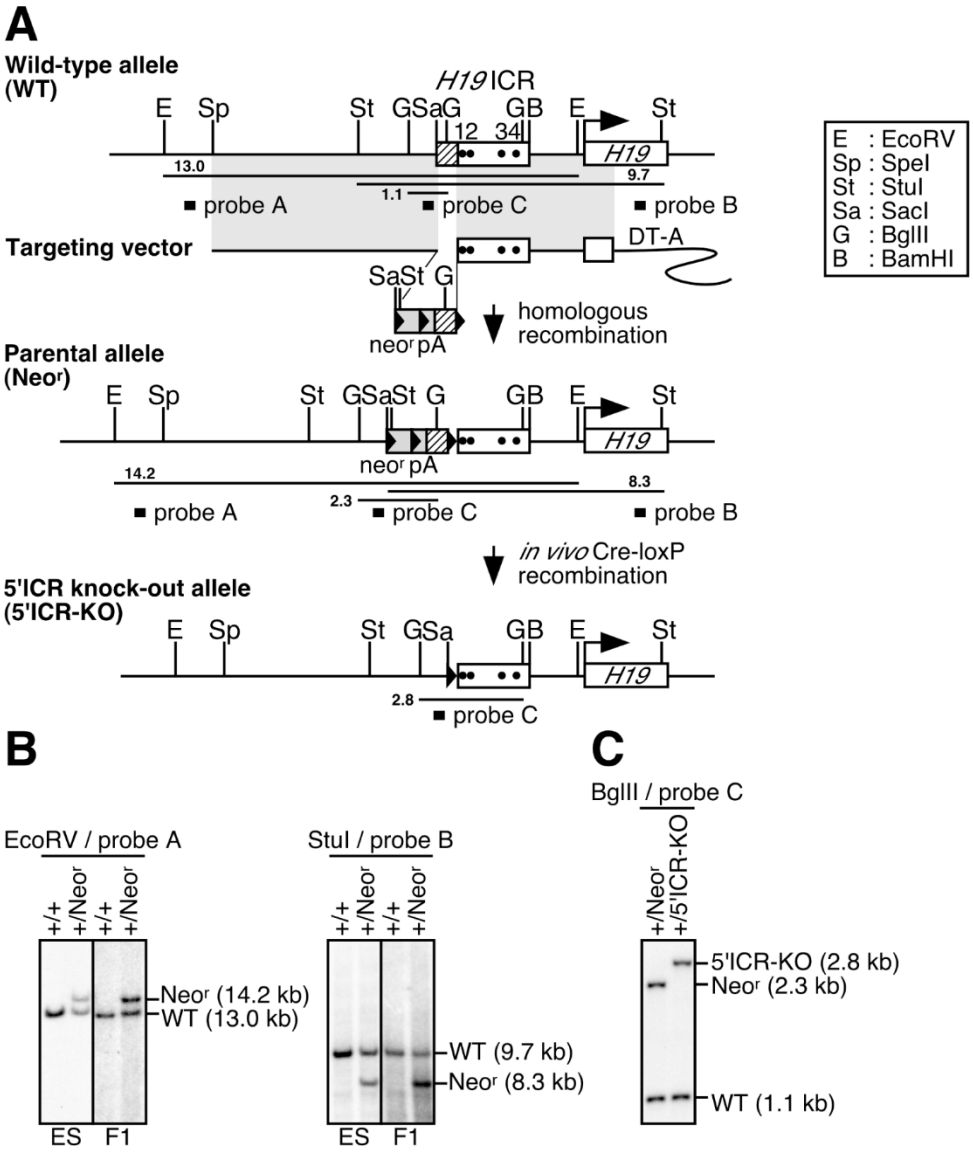

Fig. S7. Generation of 5' imprinting control region knockout (5'ICR-KO) mice

(A) Targeting strategy at the *H19* locus. Maps of the wild-type allele (WT), the targeting vector, the correctly targeted allele [Parental allele (Neo^r)], and the targeted alleles after *in vivo* Cre-loxP recombination (5'ICR-KO)) are shown from top to bottom. The solid triangles indicate the loxP sequences. The probes used for Southern blot analysis in (B) and (C) are shown as filled rectangles. The positions of restriction enzyme sites, and the expected restriction enzyme fragments and their sizes are shown next to each map.

(B) Genomic DNA from ES clones and the tails of mutant mice was digested with *Eco*RV (left) or *Stu*I (right) and separated on agarose gels, and Southern blots were hybridized to probes A or B, respectively.

(C) Genomic DNA from tail of mutant mice before or after *in vivo* Cre-loxP recombination was digested with *Bgl*II and separated on agarose gels, and Southern blots were hybridized to the probe C.

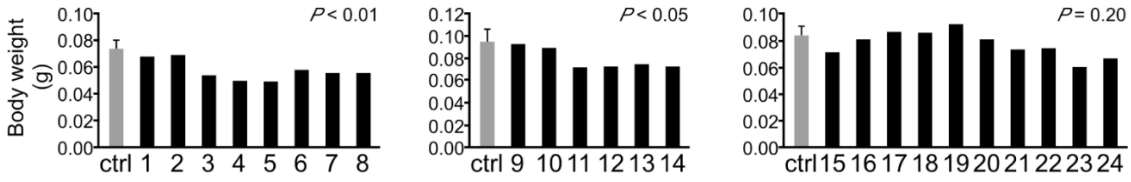

Fig. S8. A role of the 5'-region of the endogenous *H19* ICR in embryonic growth

Body weight of control (ctrl, WT/WT) and hetero-KO (WT/KO^{pat}) E12.5 embryos. The sample numbers correspond to those in Fig. 7A, B. For control embryos, the mean ± SD is shown. The differences in the means between control and KO embryos were tested using an unpaired t-test.

Supplementary Materials and Methods

Generation of insulated *H19* ICR knock-in mice

Targeting vector

Tandem chicken HS4 core sequences – Two types of DNA fragments (*Bgl*II-*Bsp*EI and *Bsp*EI-*Bam*HI), each carrying two copies of the chicken HS4 core sequences (238 bp) in tandem arrays (cHS4x2), were PCR-generated using the pBluescriptG/cHS4 double (Okamura et al., 2013a) as a template and two combinations of primer sets as follows: cHS4core-5S2, 5'-AGCCCCAGATCTCACGGGGACAGCCCCC-3' (*Bgl*II site underlined) and cHS4core-3A-BspEI, 5'-ACTAGTGGATCCGGATTCCCCGTATC-3' (*Bam*HI/*Bsp*EI); cHS4core-5S2-BspEI, 5'-AGCCCCAGATCTCCGGAGGACAGCCCCC-3' (*Bgl*II/*Bsp*EI) and cHS4core-3A, 5'-ACTAGTGGATCCTTTTTCCCCGTATC-3' (*Bam*HI). These fragments were digested with *Bgl*II/*Bsp*EI and *Bsp*EI/*Bam*HI, respectively.

Floxed neomycin^r sequence – To facilitate the cloning procedure, the following oligonucleotides were annealed (generating *Sac*II-*Pac*I-*Nde*I-*Afl*II-*Xba*I-*Nhe*I-*Bgl*II-*Sal*I sites) and replaced with *Sac*II-*Sal*I portion of the pROSA26-1 (generous gift from Dr. Soriano) (Soriano, 1999) to generate pDT-MCS: 5'-GGTTAATTAACATATGCTTAAGTCTAGAGCTAGCAGATCTG-3' and 5'-TCGACAGATCTGCTAGCTCTAGACTTAAGCATATGTTAATTAACCGC-3'.

Following this, two sets of oligos were annealed and inserted into the *Xho*I and

*Bam*HI sites, respectively, of pMC1neopA (Stratagene) to generate pMC1neopA_5'/3'-loxP: ICI-06-5S and 3A: 5'-TCGATCTAGACCCGGG*ATAACTTCGTATAATGTATGCTATACGAAGTTAT*-3' and 5'-TCGA*ATAACTTCGTATAGCATACATTATACGAAGTTAT*CCCGGGTCTAGA-3' (*Xba*I/*Sma*I); ICI-07-5S&3A: 5'-GATC*ATAACTTCGTATAATGTATGCTATACGAAGTTAT*GCGGCCGCTAGC-3' and 5'-GATCGCTAGCGGCCGC*ATAACTTCGTATAGCATACATTATACGAAGTTAT*-3' (*Not*I/*Nhe*I). The loxP sequences are italicized in each oligo. Then, the floxed neomycin resistance gene (flNeo^r) sequence was released from this plasmid by *Xba*I/*Nhe*I digestion and inserted into the *Xba*I/*Nhe*I site of pDT-MCS to generate pDT-MCS-Neo. The flNeo^r sequence, recovered as a *Sma*I-*Sal*I fragment, was ligated with a *Sma*I/*Sal*I-digested pBluescriptII KS(+), from which the flNeo^r sequence was released as a *Bam*HI-*Bgl*II fragment.

A 5'-homology/floxed Neo^r/cHS4x2 sequence – A 5' flanking sequence of the *H19* ICR [nucleotides 125,933–134,277 (AC013548; GenBank)] was recovered from a mouse BAC clone (RP23-209O22) by digestion with *Spe*I/*Bsp*EI and ligated with the S*pe*I/*Bsp*EI-digested modified pGEM-T Easy vector (carrying BspEI site between two EcoRI sites) to generate p5'hom(*Spe*I-*Bsp*EI). The *Bam*HI-*Bsp*EI portion [nucleotides 126,755–134,277 (AC013548)] of this plasmid was replaced with the inverted cHS4x2 (*Bam*HI-*Bsp*EI) fragment to generate p5'hom(*Spe*I-*Bam*HI)/cHS4x2. The flNeo^r fragment

(*Bam*HI-*Bgl*II) was then inserted into the *Bam*HI site of this plasmid to generate p5'hom(*Spe*I-*Bam*HI)/flNeo^r/cHS4x2. Following this, the *Bgl*II-*Bam*HI portion [nucleotides 126,424–126,754 (AC013548)] of this plasmid was replaced with a 5' flanking *H19* ICR sequence [*Bgl*II-*Bgl*II, nucleotides 131,759–132,884 (AC013548)] to generate p5'hom(*Spe*I-*Bgl*II/*Bgl*II-*Bgl*II)/flNeo^r/cHS4x2. Then, another 5' flanking *H19* ICR sequence [*Bgl*II-*Bgl*II, nucleotides 126,424–131,758 (AC013548)] was inserted at the *Bgl*II site of this plasmid to generate p5'hom/flNeo^r/cHS4x2. A 5'-homology [nucleotides 125,933–132,884]/floxed Neo^r/cHS4x2 fragment was prepared from this plasmid by digestion with *Spe*I and *Bsp*EI.

cHS4x2-3' homology sequence – A 3' flanking sequence of the *H19* ICR [nucleotides 134,278–144,403 (AC013548)] was recovered from a mouse BAC clone (RP23-209O22) by digestion with *Spe*I/*Bsp*EI and ligated with the *Spe*I/*Bsp*EI-digested, above mentioned, modified pGEM-T Easy vector to generate p3'hom(*Bsp*EI-*Spe*I). The *Bsp*EI-*Bgl*II portion [nucleotides 134,278– 135,261 (AC013548)] of this plasmid was replaced with the inverted cHS4x2 (*Bsp*EI-*Bgl*II) fragment to generate pcHS4x2/3'hom. The cHS4x2/3'-homology [nucleotides 135,262–138,905] fragment was prepared from this plasmid by digestion with *Bsp*EI and *Nar*I.

2.4 kb H19 ICR fragment – The oligonucleotide, 5'-CCGGGATCCAGATCTGGATC-3', was annealed (generating *Xma*I-*Bam*HI-*Bgl*II-*Bam*HI-*Xma*I sites), phosphorylated, and ligated with the *Xma*I-digested pBluescriptII KS(+) to generate pXmaI-B-G-B-XmaI. The

H19 ICR sequence in the 2.4-kb *Bgl*II fragment [nucleotides 1,127–3,503 (AF049091; GenBank)] was inserted at the *Bgl*II site of the pXmaI-B-G-B-XmaI and then released by *Xma*I digestion of the plasmid.

Backbone vector for negative selection – A double-stranded oligonucleotide carrying *Xho*I-*Spe*I-*Bsp*EI-*Nar*I-*Xma*I sites in this order was phosphorylated and ligated with the *Sal*I/*Xma*I-digested pMCDT-A(A+T/pau) (Yagi et al., 1993). The resultant plasmid was digested with *Bsp*EI/*Nar*I and ligated with the cHS4x2/3'-homology fragment (*Bsp*EI-*Nar*I) to generate pMCDT-A/cHS4x2/3'hom. This plasmid was then digested with *Spe*I/*Bsp*EI and ligated with the 5'-homology/floxed Neo^r/cHS4x2 fragment (*Spe*I-*Bsp*EI) to generate pMCDT-A/5'hom/flNeo^r/cHS4x2/cHS4x2/3'hom. Finally, this plasmid was digested with *Bsp*EI and ligated with the 2.4-kb *H19* ICR (*Xma*I) fragment to generate pMCDT-A/5'hom/flNeo^r/cHS4x2/*H19* ICR/cHS4x2/3'hom. This plasmid, termed the endo_insulated_ICR TAG vector, was linearized with *Spe*I and used for homologous recombination in ES cells. In each cloning step, the correctness of DNA construction was confirmed by DNA sequencing.

Gene targeting in ES cells and generation of mutant mice

R1 ES cells were grown on embryonic fibroblast feeder cells. Following electroporation of cells with a linearized targeting vector (Bio-Rad GenePulser Xcell at setting of 250 V and 500 microfarads), cells were selected in 0.4 mg/ml G418. Homologous

recombination in ES cells was confirmed by Southern blotting with several combinations of restriction enzymes and probes. Chimeric mice were generated by a coculture method using eight-cell embryos from CD1 mice (ICR, Charles River Laboratories). Chimeric males were bred with CD1 females, and germ line transmission of the mutant allele was identified by Southern blot analysis. TgM ubiquitously expressing Cre recombinase (Yu et al., 1998) were mated with knock-in mice to excise *neo*^{r} sequences. Successful Cre-loxP recombination was confirmed by Southern blotting.

Generation of ICR432 and ICR4321S YAC-TgM

Preparation of the targeting construct and homologous recombination in yeast

Two oligonucleotides, 5'-GATCCCGGGGTACCGATATCAGATCTGTAC-3' and 5'-AGATCTGATATCGGTACCCCGG-3', were phosphorylated, annealed (generating *Bam*HI-*Kpn*I-*Eco*RV-*Bgl*II sites) and ligated to *Bam*HI/*Kpn*I-digested pBluescriptII/KS(+) to generate pBSK-BKpEvBg(Kp), by which the original *Kpn*I site was disrupted. The following double-stranded oligonucleotide (only the upper-strand sequences are shown) was subcloned into the *Eco*RV site of pBSK-BKpEvBg(Kp) to generate the pBSK-BKpEvBg(Kp)/loxP2272-5171 plasmid:

5'-AAATAAGCTT*ATAACTTCGTATAGGATACTTTATACGAAGTTAT*CCCGGGGATAT*C**ATAACTTCGTATAGTACACATTATACGAAGTTAT***GTTAACTAC-3'

(*Hin*dIII-loxP2272-*Sma*I-*Eco*RV-loxP5171-*Hpa*I; restriction enzyme sites are underlined,

and loxP sequences are italicized).

The "ICR432" fragment, prepared from the pHS1/loxPw+/*ICR* plasmid (Tanimoto et al., 2005) by digestion with *Kpn*I [at nucleotide 1,777 (AF049091; GenBank)] and *Bam*HI (at nucleotide 3,696), was ligated with the *Bam*HI/*Kpn*I-digested pBSK-BKpEvBg(Kp)/loxP2272-5171 to generate the pBSK-loxP2272-5171/ICR432 plasmid. The ICR432-loxP2272-5171 fragment was recovered from this plasmid by *Bam*HI/*Bgl*II digestion.

A 187-bp *H19* ICR fragment [containing nucleotides 1,604–1,782 (AF049091; GenBank)] carrying CTCF site 1 was generated by PCR with the following primers and the pHS1/loxPw+/*ICR* plasmid (Tanimoto et al., 2005) as a template: 5'del_fr-5S, 5'-CGCGGATCCCGGGGTACCAGCCTAGAAAATGC-3' (*Bam*HI and *Kpn*I sites underlined) and 5'del_fr-3A, 5'-GGAAGATCTACGCGGGAGTTGCCGCGTG-3' (*Bgl*II site is underlined). The fragment was subsequently digested by *Bam*HI/*Bgl*II.

The yeast-targeting vector, pHS1/loxP5171-2272, carrying a human β-globin HS1 fragment [nucleotides 13,299–14,250 (HUMHBB; GenBank)], in which loxP5171 and loxP2271 sequences are introduced into the *Hin*dIII site [at nucleotide 13,769 in HUMHBB], was described elsewhere (Okamura et al., 2013b). A 187-bp *H19* ICR fragment was ligated to *Bam*HI-digested pHS1/loxP5171-2272 to generate pHS1-loxP5171-2272/ICR(B-Bg187). The resultant plasmid was digested with *Bam*HI/*Kpn*I and ligated with the ICR432 (*Bam*HI-*Kpn*I) fragment to generate

pHS1-loxP5171-2272/ICR4321S. Finally, the plasmid was digested with *Bam*HI and ligated with the ICR432-loxP2272-5171 (*Bam*HI-*Bgl*II) fragment to generate pHS1/ICR432-ICR4321S. In each cloning step, the correctness of DNA construction was confirmed by DNA sequencing.

The targeting vector was linearized with *Spe*I [at nucleotide 13,670 in HUMHBB] and used to mutagenize the human β-globin YAC (A201F4.3) (Tanimoto et al., 1999). Successful homologous recombination in yeast was confirmed by Southern blot analyses with several combinations of restriction enzymes and probes.

Generation of YAC-TgM

Purified YAC DNA was microinjected into fertilized mouse eggs from CD1 (ICR) mice. Tail DNA from founder offspring was screened first by PCR, followed by Southern blotting. Structural analysis of the YAC transgene was performed as described elsewhere (Tanimoto et al., 1999; Tanimoto et al., 2000). TgM ubiquitously expressing Cre recombinase were mated with ICR432-ICR4321S YAC-TgM to generate ICR432 and ICR4321S TgM sublines. Successful Cre-loxP recombination was confirmed by Southern blotting.

Generation of 5'ICR knockout mice

Targeting vector

A "loxP/1126-1603/loxP" fragment [657-bp, *H19* ICR, nucleotides 1,099–1,640 (AF049091; GenBank) containing two *loxP* sites] was generated by PCR with the following primers and the murine *H19* ICR DNA as a template: 443ORI-5S1, 5'-AAAA-CTCGAG (*Xho*I)-ACTAGT (*Spe*I)-gcatgcctaacttgtttctggaagaag-*ATAACTTCGTATAGCATACATTATACGAAGTTAT*-GTCGAC(*Sal*I)-agatctagctctatcccatcg aaa-3' and 443ORI-3A1, 5'-TCCC-CCCGGGCGCC (*Xma*I/*Nar*I)-TCCGGA (BspEI)-atcgattttgctgccaccacgcggcaactcccgcgta-*ATAACTTCGTATAATGTATGCTATACGAAGTTAT* -AAGCTT (*Hin*dIII)-aaaccccacaactgattcagcag-3'. Nucleotides in lower case letters are from *H19* ICR sequences. Restriction enzyme sites and *loxP* sequences are underlined and italicized, respectively. Following *Xho*I and *Xma*I digestion, the fragment was ligated with the *Sal*I/*Xma*I-digested pMCDT-A(A+T/pau) (Yagi et al., 1993) to generate pMCDT-A/loxP/1126-1603/loxP.

The 5' portions of the right [*Cla*I-*Bsp*EI, nucleotides 133,395–134,277 (AC013548.13; Genbank)] and left arm [*Spe*I-*Sph*I, nucleotides 125,933–132,861] fragments, excised from the pRP23-209O22 BAC clone, were introduced into the *Cla*I/*Bsp*EI and *Spe*I/*Sph*I sites, respectively, of the pMCDT-A/loxP/1126-1603/loxP to generate pMCDT-A/LA/loxP/1126-1603/loxP/5'-RA.

A "loxP/839-1229" fragment [445 bp, containing a *loxP* site and *H19* ICR sequences, nucleotides 839–1,229 (AF049091)] was generated by PCR with the following primers and the murine *H19* ICR DNA as a template: 5'ICR-KO-5S1, 5'-AA-GAGCTC

(*Sac*I)-GGATCC (*Bam*HI)-*ATAACTTCGTATAGCATACATTATACGAAGTTAT*-GTCGAC (*Sal*I)-tttctccaccacttgt-3' and 5'ICR-KO-3A1, 5'-cagcacttttgactgcattg-3'. A "loxP/839-1126" fragment [*H19* ICR, nucleotides 839–1,126 (AF049091)], generated by digestion of the loxP/839-1229 fragment with *Sac*I and *Bgl*II, and a "1127-1603/loxP/1604-1640" fragment [containing *H19* ICR sequences, nucleotides 1,127–1,603 and 1,604–1,640 (AF049091), and a loxP site in between], released from the pMCDT-A/loxP/1126-1603/loxP by digestion with *Bgl*II and *Cla*I, were ligated and replaced with *Sac*I-*Cla*I portion of the pMCDT-A/LA/loxP/1126-1603/loxP/5'-RA to generate pMCDT-A/LA/loxP/839-1603/loxP/5'-RA.

The 3' portion of the right arm [*Bsp*EI-*Nar*I, nucleotides 134,278–138,906 (AC013548.13)] fragment excised from the pRP23-209O22 BAC clone was ligated with *Bsp*EI/*Nar*I-digested pMCDT-A/LA/loxP/839-1603/loxP/5'-RA to generate pMCDT-A/LA/loxP/839-1603/loxP/RA.

A "*loxP*/pA" fragment was generated by PCR with the following primers using pMC1neo-polyA (Stratagene) as a template: loxP-pA-5S1, 5'-GA-AGATCT (*Bgl*II)-*ATAACTTCGTATAGCATACATTATACGAAGTTAT*-GGATCGGCAATAAAAAGACA -3' and Reverse, 5'-GGAAACAGCTATGACCATG-3'. Following *Bgl*II and *Sal*I digestion, the fragment was ligated with the *Bam*HI/*Sal*I-digested pMC1neo plasmid to generate pMC1neo/loxP/pA. A "neo/loxP/pA" fragment, released from this plasmid by *Xho*I and *Sal*I digestion was ligated with *Sal*I-treated pMCDT-A/LA/loxP/839-1603/loxP/RA to

generate a targeting vector, pMCDT-A/LA/loxP/neo/loxP/pA/839-1603/loxP/RA. In this plasmid, *H19* ICR sequences from nucleotides 839 to 1,603 [765 bp (AF049091)] are flanked by a set of loxP sites. In each cloning step, the correctness of DNA construction was confirmed by DNA sequencing. The targeting vector was linearized with *Spe*I and used for homologous recombination in ES cells.

Gene targeting in ES cells and generation of mutant mice were performed as described previously.

Stella knockout mice

The *Stella* (*PGC7*) knockout mouse strain (RBRC01494) (Nakamura et al., 2007) was provided by RIKEN BRC through the National Bio-Resource Project of the MEXT, Japan.

Combined bisulfite restriction analysis (COBRA)

Genomic DNA extracted from sperm was treated with sodium bisulfite using the EZ DNA Methylation Kit according to the manufacturer's instructions (Zymo Research). The endogenous and transgenic ICRs were amplified by nested PCR, and the aliquots of PCR products were digested with *Taq*I enzyme and subjected to polyacrylamide gel electrophoresis. After ethidium bromide staining of the gels, photos were taken, and the white and black aspects of the image were reversed to facilitate DNA band recognition.

RT-qPCR

The total RNA of oocytes and preimplantation embryos was extracted with ISOGEN (Nippon Gene) and converted to cDNA using ReverTra Ace qPCR RT Master Mix with gDNA Remover (TOYOBO). Quantitative amplification of cDNA was performed with the Thermal Cycler Dice (TaKaRa Bio) using SYBR Premix EX TaqII (TaKaRa Bio) and PCR primers listed in a table.

DNA methylation analysis by Southern blotting

Genomic DNA from insulated *H19* ICR knock-in mice or ICR432 TgM was first digested by *Bam*HI and *Bgl*II or *Eco*T22I, respectively, to liberate the *H19* ICR region and then subjected to the methylation-sensitive enzymes *Hha*I or *Bst*UI, respectively. Following size separation by agarose gel electrophoresis, Southern blots were hybridized with the α-^{32}P-labeled probes and subjected to X-ray film autoradiography.

Lists of primers used in this study

Table S1. Primer sets for bisulfite sequencing analysis

	allele	regions analyzed	PCR round	5' primer	3' primer
nested PCR	endogenous (wild-type)	I	1st	ICR-MA-5S1	ICR-MA-3A3
			2nd	ICR-MA-5S2	ICR-MA-3A1
	transgene (ICR)	I	1st	ICR-MA-5S1	BGLB-MA-3A1
			2nd	ICR-MA-5S2	ICR-MA-3A1
	transgene (ICR)	I'	1st	ICR-MA-5S13	BGLB-MA-3A2
			2nd	ICR-MA-5S13	ICR-MA-3A2
	transgene (ICR)	II	1st	LCR-MA-5S1	ICR-MA-3A6
			2nd	ICR-MA-5S4	ICR-MA-3A5
	transgene (ICR4321S)	VI	1st	ICR-MA-5S10	BGLB-MA-3A1
			2nd	ICR-MA-5S1	BGLB-MA-3A2
	transgene (ICR432)	VI'	1st	ICR-MA-5S10	BGLB-MA-3A1
			2nd	ICR-MA-5S1	BGLB-MA-3A2
	transgene (ICR4321S, ICR432)	VII	1st	LCR-MA-5S1	ICR-MA-3A15
			2nd	ICR-MA-5S4	ICR-MA-3A14
single-round PCR	Insulated	III		ICR-MA-5S13	3'cHS4-MA-3A1
	Insulated	IV		ICR-MA-5S2	ICR-MA-3A17
	wild-type	IV'		ICR-MA-5S2	ICR-MA-3A21
	Insulated	V		cHS4-MA-5S1	ICR-MA-3A15
	wild-type	V'		ICR-MA-5S20	ICR-MA-3A15
	5'ICR-KO	VIII		ICR-MA-5S16	ICR-MA-3A23
	wild-type	VIII'		ICR-MA-5S16	ICR-MA-3A24

Table S2. Primer sequences for bisulfite sequencing analysis

	name	sequences
5' primer	ICR-MA-5S1	5'- gaatttgaggattatgtttagtgg -3'
	ICR-MA-5S2	5'- ttaaggattagtatgaatttttgg -3'
	ICR-MA-5S4	5'- gaatttggggtatttaaagttttg -3'
	ICR-MA-5S10	5'- gtttgatgtaggatttttttagttg -3'
	ICR-MA-5S13	5'- ggtgatttatagtattgttatttg -3'
	ICR-MA-5S16	5'- tatatgtattggtttatggggttt -3'
	ICR-MA-5S20	5'- gggatattgtaatggttgaatttt -3'
	LCR-MA-5S1	5'- tatagatgttttagttttaataag -3'
	cHS4-MA-5S1	5'- attgagtttggattgaatagatttta -3'
3' primer	ICR-MA-3A1	5'- aacataacaatactataaccatac -3'
	ICR-MA-3A2	5'- aacaatactaaatctacctaaaac -3'
	ICR-MA-3A3	5'- tttatccaaatactaaataacacc -3'
	ICR-MA-3A5	5'- aacttaactcattccctacacaac -3'
	ICR-MA-3A6	5'- atatacacctctaaaataattccc -3'
	ICR-MA-3A14	5'- aaaacataaaaactattatataca -3'
	ICR-MA-3A15	5'- accaaccaatataactcactataa -3'
	ICR-MA-3A17	5'- aactttaaaaaaaaactatcctcc -3'
	ICR-MA-3A21	5'- acttactaccctcattatacttt -3'
	ICR-MA-3A23	5'- cactctctctatactcattcttta -3'
	ICR-MA-3A24	5'- aaaaaccataccctattcttaaac -3'
	BGLB-MA-3A1	5'- tctcgtcaaaccaccttcattaac -3'
	BGLB-MA-3A2	5'- ttctaaccccacaaaaatttattc -3'
	3'cHS4-MA-3A1	5'- acttatttctaaaaaaaaaaatcccc -3'

Table S3. Primer sets for RT-qPCR analysis

gene		primer name	sequences	reference
Dnmt3l	5' primer	3L-5S1	5'- gtgcgggtactgagccttttaga -3'	(La Salle et al., 2004)
	3' primer	3L-3A1	5'- cgacatttgtgacatcttccacgta -3'	
Dnmt3a	5' primer	3a-ex17F	5'- tccgcagcgtcacacagaagcat -3'	
	3' primer	3a-ex18R	5'- gcgggcagggttgacaatggagagg -3'	
Dnmt3b	5' primer	3b-ex19F	5'- gcaatgatctctctaacgtcaatcc -3'	
	3' primer	3b-ex20R	5'- gggcgggtataattcagcaagtgg -3'	
H2afz	5' primer	mH2afz-F	5'- acagcgcagccatcctggagta -3'	(Mamo et al., 2007)
	3' primer	mH2afz-R	5'- ttcccgatcagcgatttgtgga -3'	
Igf2	5' primer	mIgf2-5S	5'- aggggagcttgttgacacg -3'	(Kono et al., 2004)
	3' primer	mIgf2-3A	5'- gggtatctggggaagtcgtc -3'	
H19	5' primer	mH19-5S	5'- catgtctgggcctttgaa -3'	(Kono et al., 2004)
	3' primer	mH19-3A	5'- ttggctccaggatgatgt -3'	
GAPDH	5' primer	mGAPDH-5S	5'- aaaatggtgaaggtcggtgtg -3'	
	3' primer	mGAPDH-3A	5'- tgaggtcaatgaaggggtcgt -3'	

Supplementary References

Kono, T., Obata, Y., Wu, Q., Niwa, K., Ono, Y., Yamamoto, Y., Park, E. S., Seo, J. S. and Ogawa, H. (2004). Birth of parthenogenetic mice that can develop to adulthood. *Nature* **428**, 860-864.

La Salle, S., Mertineit, C., Taketo, T., Moens, P. B., Bestor, T. H. and Trasler, J. M. (2004). Windows for sex-specific methylation marked by DNA methyltransferase expression profiles in mouse germ cells. *Dev Biol* **268**, 403-415.

Mamo, S., Gal, A. B., Bodo, S. and Dinnyes, A. (2007). Quantitative evaluation and selection of reference genes in mouse oocytes and embryos cultured in vivo and in vitro. *BMC developmental biology* **7**, 14.

Nakamura, T., Arai, Y., Umehara, H., Masuhara, M., Kimura, T., Taniguchi, H., Sekimoto, T., Ikawa, M., Yoneda, Y., Okabe, M., et al. (2007). PGC7/Stella protects against DNA demethylation in early embryogenesis. *Nat Cell Biol* **9**, 64-71.

Okamura, E., Matsuzaki, H., Fukamizu, A. and Tanimoto, K. (2013a). The chicken HS4 insulator element does not protect the H19 ICR from differential DNA methylation in yeast artificial chromosome transgenic mouse. *PloS one* **8**, e73925.

Okamura, E., Matsuzaki, H., Sakaguchi, R., Takahashi, T., Fukamizu, A. and Tanimoto, K. (2013b). The H19 imprinting control region mediates preimplantation imprinted methylation of nearby sequences in yeast artificial chromosome transgenic mice. *Mol Cell Biol* **33**, 858-871.

Soriano, P. (1999). Generalized lacZ expression with the ROSA26 Cre reporter strain. *Nat Genet* **21**, 70-71.

Tanimoto, K., Liu, Q., Bungert, J. and Engel, J. D. (1999). The polyoma virus enhancer cannot substitute for DNase I core hypersensitive sites 2-4 in the human beta-globin LCR. *Nucleic Acids Res* **27**, 3130-3137.

Tanimoto, K., Liu, Q., Grosveld, F., Bungert, J. and Engel, J. D. (2000). Context-dependent EKLF responsiveness defines the developmental specificity of the human epsilon-globin gene in erythroid cells of YAC transgenic mice. *Genes Dev* **14**, 2778-2794.

Tanimoto, K., Shimotsuma, M., Matsuzaki, H., Omori, A., Bungert, J., Engel, J. D.

and Fukamizu, A. (2005). Genomic imprinting recapitulated in the human beta-globin locus. *Proc Natl Acad Sci U S A* **102**, 10250-10255.

Yagi, T., Nada, S., Watanabe, N., Tamemoto, H., Kohmura, N., Ikawa, Y. and Aizawa, S. (1993). A novel negative selection for homologous recombinants using diphtheria toxin A fragment gene. *Analytical biochemistry* **214**, 77-86.

Yu, R. N., Ito, M., Saunders, T. L., Camper, S. A. and Jameson, J. L. (1998). Role of Ahch in gonadal development and gametogenesis. *Nat Genet* **20**, 353-357.